Thermodynamic analysis of a concentrated solar energy desalination plant

Piotr Przemysław Mazur

Thesis to obtain the Master of Science Degree in

Energy Engineering and Management

Supervisor: Prof. Pedro Jorge Martins Coelho

Prof. Miguel Abreu de Almeida Mendes

Examination Committee

Chairperson: Prof. Edgar Caetano Fernandes

Supervisor: Prof. Pedro Jorge Martins Coelho

Member of the Committee: Prof. Luís Filipe Moreira Mendes

October 2021

Abstract

In this thesis, a concentrated solar energy desalination plant is analysed. Desalination process is a chance to bring fresh water to regions with access only to seawater and the use of solar energy minimises the carbon footprint of this energy intensive process. The aim is to perform a thermodynamic analysis and observe the behaviour of the system with considered location in Saudi Arabia and the Red Sea as the seawater source. A review of available systems is performed resulting in the choice of a solar tower with thermal storage and a multi-effect distillation as a best fit for the requirements of the system. A model for each part of the system is developed based on literature and validated for correct implementation. The entire model is used to perform a simulation of operation over one year. A strong variation of some parameters within hours requires a part of the model to perform calculation on an hourly basis. The results show a high variation of fresh water produced depending on the month, mainly influenced by the temperature of the seawater. The variation of the direct normal irradiance impacts the amount of solar power collected and requires a large storage tank to allow for a continuous operation of the system. The concentrated solar energy desalination system is a chance for a fresh water source, but it still has its problems, mainly resulting from the changing weather conditions and large thermal storage tank requirements.

Keywords: concentrated solar energy; desalination; system modelling; solar tower; thermal storage; central receiver;

Resumo

Nesta tese, é analisada uma central de dessalinização de energia solar concentrada. O processo de dessalinização traz a oportunidade de trazer água doce para regiões com acesso apenas à água do mar e por sua vez a utilização de energia solar minimiza a pegada ecológica deste processo energeticamente intenso. O objectivo é realizar uma análise termodinâmica e observar o comportamento do sistema numa localização na Arábia Saudita e utilizar o Mar Vermelho como fonte de água do mar. É efectuada uma análise dos sistemas disponíveis, resultando na escolha de uma torre solar com armazenamento térmico e uma destilação de múltiplo efeito como melhor adaptação aos requisitos do sistema. Um modelo para cada parte do sistema é desenvolvido com base em literatura e validado para uma implementação correta. O modelo completo é utilizado para realizar uma simulação de funcionamento durante um ano. Uma alta variação de alguns parâmetros num curto espaço de horas requer uma parte do modelo que efetue os cálculos em períodos de horas. Os resultados mostram uma grande variação de água doce produzida em função do mês, principalmente influenciada pela temperatura da água do mar. A variação da irradiação solar tem impacto na quantidade de energia solar recolhida que faz com que seja necessário um grande tanque de armazenamento para permitir um funcionamento contínuo do sistema. O sistema de dessalinização alimentado a energia solar concentrada é uma oportunidade para obter água doce, mas ainda tem os seus problemas, resultantes principalmente da mudança das condições meteorológicas.

Palavras-chave: energia solar concentrada; dessalinização; modelação de sistemas; torre solar; armazenamento térmico; receptor central;

Contents

List of figures

List of tables

List of acronyms

CSE   Concentrated solar energy

DNI   Direct normal irradiance

MENA   Middle East and North Africa

MSF   Multi-stage flash

MED   Multi-effect distillation

HTF   Heat transfer fluid

HTC   Heat transfer coefficient

Nomenclature

$\dfrac{d_x}{H_{to}}$	elemental length of north-south ratio	$-$	Nu	Nusselt number	$-$
$\dfrac{d_y}{H_{to}}$	elemental length of east-west ratio	$-$	P	power	W
L_c	characteristic dimension	$-$	PD	packing density	$-$
N_f	points in the field boundary	m	Pr	Prandtl number	$-$
P_t	tube pitch	m	Q	energy stored	J
$\dot{Q}$	rate of heat transfer	W	R	thermal resistance	$\dfrac{m^2 \cdot K}{W}$
c_p	specific heat	$\dfrac{J}{kg \cdot K}$	Ra	Rayleigh number	$-$
$\dot{m}$	mass flow rate	$\dfrac{kg}{s}$	Re	Reynolds number	$-$
$\dot{q}$	heat flux	$\dfrac{W}{m^2}$	Ri	Richardson number	$-$
$\dfrac{r}{H_{to}}$	ratio of radial distance from the solar tower	$-$	S	slant height	km
$\dfrac{x}{H_{to}}$	ratio of north-south distance to tower height	$-$	T	temperature	$°C$
$\dfrac{y}{H_{to}}$	ratio of east-west distance to tower height	$-$	U	overall heat transfer coefficient	$\dfrac{W}{m^2 \cdot K}$
h	heat transfer coefficient	$\dfrac{W}{m^2 \cdot K}$	e	power per mirror area	$\dfrac{W}{m^2}$
$hour$	hour of day	h	f	friction factor	$-$
A	area	m^2	g	gravitational acceleration	$\dfrac{m}{s^2}$
B	baffle spacing	m	k	thermal conductivity	$\dfrac{W}{m \cdot K}$
BPE	boiling point elevation	K	lat	latitude	$°$
C, m, n, b	coefficients	$-$	no	amount	$-$

D	diameter	m	r	radius	m
DNI	Direct Normal Irradiation	$\dfrac{W}{m^2}$	ref	reflectivity	$-$
Gr	Grashof number	$-$	t	time	h
H	height	m	w	velocity	$\dfrac{m}{s}$
I	specific enthalpy	$\dfrac{J}{kg}$	x	salinity	$\dfrac{g}{kg}$
L	length of a tube	m			

Greek letters

Δ	difference/increment	var
δ	thickness	m
ρ	density	$\dfrac{kg}{m^3}$
μ	dynamic viscosity	$Pa \cdot s$
β	coefficient of volumetric expansion	$\dfrac{1}{K}$
ϵ	emissivity	$-$
σ	Stefan-Boltzmann constant	$\dfrac{W}{m^2 \cdot K}$
η	efficiency	$\%$
α	parameter for desalination	$-$
γ	parameter for desalination	$-$
λ	latent heat of evaporation	$\dfrac{J}{kg}$
θ	angle for heliostat parameters	$^\circ$

Subscripts

h	convective		j	location in the field
he	heliostat field		k	number of effect
hex	heat exchanger		l	actual annual
$hour$	hour of the day		lat	latent heat
htf	heat transfer fluid		log	logarithmic
B	brine		$loop$	water heating loop
D	distillate		$loss$	losses
F	feed		m	total annual
a	collected per square of tower height		max	maximum
abs	absorbed		$mean$	mean value
air	air		min	minimum
alt	altitude		$natural$	natural convection
amb	ambient		nd	non-dimensional
att	atmospheric attenuation		o	outer
az	azimuth		$oper$	operation
b	bottom		out	outcoming
$boil$	boiled portion of distillate		ph	pre-heater
c	conductive		re	receiver
$c1c2$	between two layers of concrete		ref	reflective
cap	rated capacity		s	surface
$conc$	concrete		sb	shadowing and blocking
$cond$	condenser		sh	shell
cos	cosine		$sens$	sensible heat
d	desalination		$soil$	soil
dec	declination		$spill$	spillage
em	radiative		st	storage
eq	equivalent		sw	seawater
ev	evaporation		sys	system
f	flow		top	top
fi	final effect		$total$	sum of all
$flash$	flashed portion of distillate		$tube$	tube
$forced$	forced convection		v	vapour
i	inner		$vent$	ventilation
i	hour of the year		w	wall
in	incoming		$water$	water (cycle) parameters
ins	insulation		z	zenith

1. Introduction

1.1. Motivation

One of the resources necessary for every human to survive is water. Although in one way we are surrounded by water, as it covers up to 70% of the Earth's surface, merely around 1% is fresh water in liquid state, which can be directly drawn and used. About 2% exists as ice caps or glaciers, and 97% is salt water in seas and oceans [1].
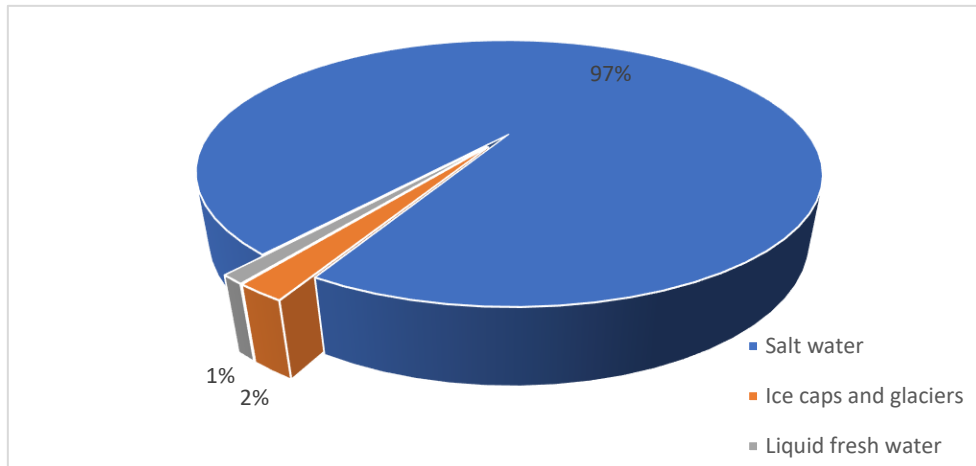
Figure 1 - Available water resources

With the Earth's growing population, it is estimated that presently over one-third of people live in countries with limited access to fresh water, and that number is expected to grow [2]. Given the high amount of salt water available, desalination became a valuable way to provide fresh water to people. Although not all countries have access to sea water, it is much more available than fresh water. Water desalination techniques have been developing for many years now and have improved by far, yes still this process carries certain problems. The main one is the high energy consumption of the process, given that the most common techniques either require evaporation of water or very high pressure in case of reverse osmosis. The use of fossil fuels naturally leads to emission of greenhouse gases and, depending on the fuel used, possibly other harmful flue gases. One way of eliminating that problem is to use renewable energy as a source for desalination plant. Considering that the regions with low fresh water reserves usually are in regions of high solar irradiance, the use of solar energy seems as the most appropriate solution. To avoid the need of lengthy transmission lines, combined solar energy and desalination plants pose an interesting solution.

1.2. Review of technologies

This part of the thesis focuses on a review of technologies, both on the side of concentrated solar energy and desalination. The focus will be put on the most mature technologies, as they are well developed and researched, but emerging solutions will also be mentioned. Based on the advantages and disadvantages of the methods, and with the intent of best fit for the requirements, a system combining concentrated solar energy and desalination will be chosen for the next step – thermodynamic system analysis.

1.2.1. Concentrated solar energy

Firstly, it should be mentioned why only concentrated solar energy technologies are considered. Nonconcentrated solutions carry some significant limitations. In case of methods such as solar stills, which are based on direct desalination, the operation is limited to small-capacity systems. With photovoltaics, only desalination techniques based on use of electricity, namely reverse osmosis, could be used. Concentrated solar energy offers a wider range of possible combinations with desalination, as it can either produce heat, or, upon coupling with proper cycle, mechanical energy or electricity. Additionally, for the Middle East and North Africa (MENA) region, which will be the main focus in this thesis, concentrated solar energy is the recommended solution, given the weather condition in the area [3].

The most common solutions for concentrated solar energy are parabolic concentrators (with either dish or trough), Fresnel lens and solar tower. Compound concentrator is a solution which uses more than one element for improvement of focus; this technology is still in development and will therefore not be considered here [4].
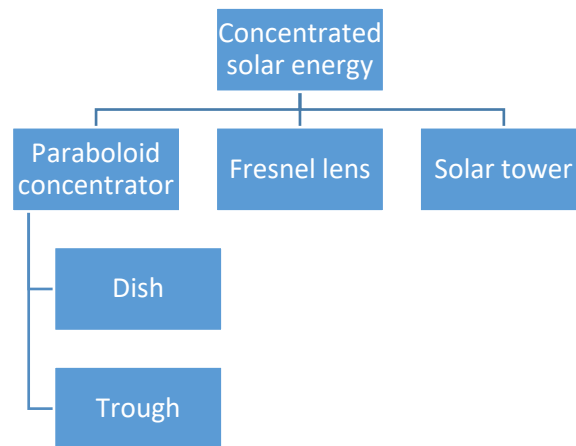
Figure 2 - Concentrated solar energy technologies

The division of CSP solutions is presented in Figure 2.

1.2.1.1. Dish paraboloid concentrator

It is a type of focal point concentrator, meaning that the solar energy is concentrated in a point (or, to be more exact, a small area), as opposed to a linear concentrator where it is concentrated on a linear tube. The mirror is of dish-like shape and allows for obtaining remarkably high temperatures due to high concentration ratio. The dimensions of the dish can vary depending on the needs and are limited mainly by the self-weight of the structure. In most cases several of such concentrators are installed instead of a large one to ease handling and manufacturing. The main advantages are easy installation and low wind resistance. It is also the oldest type of paraboloid concentrator, so technology is very mature. Despite these assets, currently it is not the preferred solution and is being dominated by trough concentrators [4]. The main reason for that is the high capital and operation costs due to a dual axis tracking system and high material demand. Dish paraboloid concentrators also exhibit some reliability problems [5].

1.2.1.2. Trough paraboloid concentrator

This is now one of the most commonly used solar concentrators. Mirrors, in the shape of trough, focus solar energy onto a linear receiver, transferring heat to the fluid inside it. Only a one-dimensional tracking system is required, and mirrors can be aligned either in east-west or north-south configuration, although for low altitude area the latter is recommended [4]. The main advantages are that the system is well-developed and well-studied, the temperature of operation is high and the tracking system is simple (since it is only one-dimensional). Unfortunately, large dimensions of the mirrors may cause problems. The wind resistance is high, requiring strong and more expensive support system, and increasing the energy consumption of the tracking system. The shape of the mirrors makes is prone to dust accumulation, which decreases the reflective properties. That issue is especially important to consider given the considered location of the plant, since in Saudi Arabia sandstorms and soiling are rather frequent [5].

1.2.1.3. Fresnel lens

Fresnel lens is considered an alternative to the previous solution. Instead of a massive trough shaped mirror, several flat (or slightly curved) mirrors are used. In this case the solar energy is also focused on a linear receiver and similar temperatures can be reached. The problems of wind resistance and difficult cleaning are eliminated. Nevertheless, other issues appear: since flat mirrors are not capable of focusing solar energy as well as curved ones, usually a second concentrator is installed around the linear receiver, increasing the overall investment cost; since it is an array of flat mirrors instead of just one, an independent tracking system is required; the optical efficiency and collection temperature are lower than in other solutions. Due to these issues, there have not been many practical large-scale applications of this system [4] [5].

1.2.1.4. Solar tower

Solar tower systems work in a different manner than the aforementioned solutions. In this case central receiver is placed on the top of a tower and a system of heliostats – usually concave or spherical - work to focus solar energy on it. Heliostats require an asynchronous two-dimensional tracking system and maintain proper distance from one another to avoid shading effects. The system provides a high concentration ratio and allows to reach high temperatures [4]. The receiver can either be direct, where reflected sunrays can directly heat the fluid, or indirect, where a tube wall is heated and from there heat is transferred to the fluid; the latter solution is more common as it can work with higher solar radiation intensity [4]. It overcomes certain issues present in the previous solutions, yet also carries some disadvantages. The asynchronous two-dimensional tracking system needs to be precise and is not that easy to control; large distance between the heliostats and receiver may cause defocus; presence of many heliostats and distance between them means a large area is required for that system.

1.2.1.5. Storage

It is important to mention the possibility of storage combined with concentrated solar energy. The heat transfer fluid used in CSP can be directly used in the combined process – desalination, power generation, or other. The problem with that solution is that the operation is completely dependent on the weather conditions and time

of the day. Application of storage allows to maintain the operation even when the sun is not shining at that moment. Thermal energy storage can be divided into three types according to method of storing heat: sensible heat, latent heat and chemical heat. Sensible heat storage uses energy stored in a liquid or solid in high temperature. Latent heat storage involves a phase change of the used material. Chemical heat is based on chemical reversible reactions [6]. The simplest and most developed one is the first option, as it only requires two single-phase tanks – one with hot fluid and one with cold fluid. In most cases the material used to store heat is molten salt, as it is characterised by high melting point temperatures (from about 130°C to 220°C) and high temperatures of thermal stability (about 550°C to 600°C) depending on the type of molten salt [7]. If such high temperatures are not required, other fluid may be applied, such as thermal oils (applicable range of temperatures is from about 0°C to 400°C) [8].

Even though storage systems make the plant more expensive and complex, and they have some heat losses to the environment, lack of dependence on the weather conditions makes them a valuable option. It is especially important when combined with desalination, as some of the technologies in that operation cannot be coupled with intermittent heat supply. Doing so would result in low economic performance, decreased lifetime of the plant, increased scaling, fouling and corrosion and overall performance decrease [3].

1.2.2. Desalination

In the field of desalination technologies, the main division is into direct systems and indirect systems. Direct methods, in which the main technologies are solar stills, solar humidification-dehumidification-desalination or solar chimneys, are recommended for small- to medium-capacity systems and are coupled with the use of unconcentrated solar energy; as for the sake of this thesis CSP is analysed, only indirect systems are considered. Among those, another division can be made, into non membrane (thermal) and membrane systems. The first, which works based on the process of evaporation and then condensation of water vapour, comprise mainly the multi-stage flash distillation, multi-effect distillation and vapour compression; the latter use membranes to remove salts from the feed and compose mainly of reverse osmosis. Membrane distillation is a combination of thermal and membrane systems. The division of desalination technologies is presented in Figure 3.
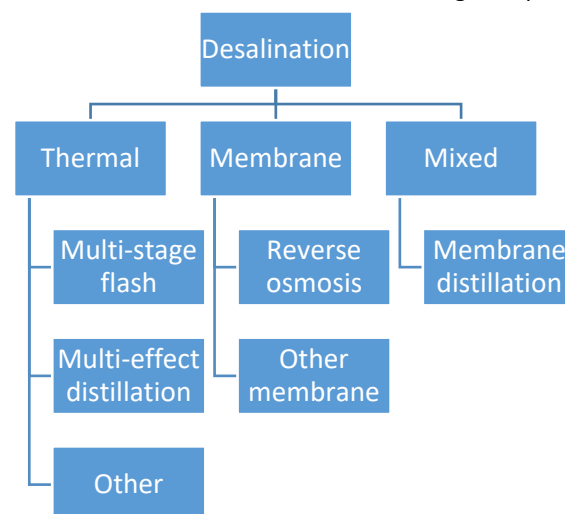

Figure 3 - Desalination technologies

1.2.2.1.   Multi-stage flash

This method is based on sudden boiling of water, which occurs once it is heated just below its boiling point and introduced into a vessel with lower pressure. Seawater is preheated in tubes flowing through the stages of the process and then heated to the desired temperature in a heat exchanger with a heat transfer fluid from solar system as hot fluid. It then enters the first stage, where proper pressure is maintained with a vacuum pump. The vapour is condensed on tubes with preheating seawater and collected on each stage. The brine enters the next stage – where even lower pressure is maintained – and the flash and condensation processes repeat [9]. The brine from the last stage is highly concentrated and can be disposed of. The number of stages vary depending on the system and can reach even 40, although in most applications it is around 20 stages [3].

It is currently the second most dominant desalination technology after reverse osmosis [4], making it also well-developed and mature. On the downside, the auxiliary equipment consumes quite a lot of energy decreasing the attractiveness of the process [10]. The requirement of high top brine temperature (entering the first stage), at the level of 90 - 120°C, is quite high to obtain when combined with solar energy as heat source for the system. It also causes issues related to fouling and scaling [4].

1.2.2.2.   Multi-effect distillation

In multi-effect distillation, vessels are also used, in this case called effects, and the method of operation is to some extent similar. Hot heat transfer fluid is the source of heat for the first effect. In all effects low pressure is maintained and seawater – usually preheated in a heat exchanger by concentrated brine – is sprayed. In the first effect the seawater evaporates due to temperature obtained from heat transfer fluid; the resulting water vapour is directed to the next effect where it acts as a heat source and condenses, after which it is collected as fresh water [11]. The process is repeated for a proper number of effects, depending on the system.

MED is becoming a more common solution as it is superior to MSF due to its lower top brine temperature being in the range of 55 - 120°C, which allows to avoid scaling and corrosion problems and is easier to obtain with solar energy as heat source. Being a thermal method, it is still energy intensive, but its overall performance can be increased by application of heat pumps to recover energy from the last effect and to reduce the heat requirements for the first effect [12].

1.2.2.3.   Other thermal

Among other processes for desalination, not involving the use of membranes, freeze desalination or adsorption can be mentioned. Freeze desalination is based on bringing seawater to temperature below its freezing point producing ice crystals of fresh water [11]. Although the operation is rather simple, the main problem is that crystals formed during the process are small. As a result, they are not easy to separate and require significant amounts of fresh water to wash them out. Because of that the efficiency is low and the cost high, resulting in no wide applications of the method [9]. Adsorption system contains mainly the evaporator, adsorption beds – usually of silica or zirconia – and condenser [11]. The system is complex and lacks large-scale tests as only theoretical or experimental studies are available, therefore it will not be considered [4]. An interesting solution

is vapour compression. The incoming seawater is heated by an external source, which can be solar energy, and allowed to flash. The vapours are compressed and used to heat the same or next stage of the process. It can either work with mechanical vapour compression MVC, where electricity is required to power the compressors, or thermal vapour compression TVC, which requires high pressure motive steam [4] [11]. Although it carries some advantages and can work as a stand-alone method, due to its low performance in practical application it is usually combined with MSF or MED for improvement of efficiency [9].

1.2.2.4. Reverse osmosis

Reverse osmosis is now the most commonly used technology in medium- and large-scale desalination [13]. It can be coupled with photovoltaics or solar thermal systems; since photovoltaics is not considered for the purpose of this thesis, only the latter will be discussed. The process is based on applying high pressure pumps to the seawater and allowed to pass through the RO membrane. The pressure applied needs to be above the osmotic pressure allowing water molecules to pass and preventing the salts from passing. The salts are drained in the form of brine and usually pass through a pressure exchanger to lower the energy needs for pumps [11]. Since this is a pressure driven, not thermally driven process, solar thermal energy cannot be directly used to run it. The recommended solution is coupling with Solar Organic Rankine Cycle. Heat transfer fluid is used in a boiler to evaporate an organic fluid, such as toluene, which is then expanded in a turbine giving out mechanical energy. It then passes through a condenser with seawater as cold fluid and goes to a pump to maintain a cycle. Mechanical energy from the turbine can be used directly to drive the high-pressure pumps for RO process. Another solution is coupling to a generator and using produced electricity to run the pumps, but it increases the investment cost and energy losses, so it is not a recommended option [11] [13].

RO is considered the most energy efficient technique for large scale, as opposed to thermal methods it does not require energy intensive evaporation of water [14]. It is also one of the most mature technologies in the field. To consider disadvantages, the main is that prior to delivering water to the RO membrane, it already needs to be relatively pure and voided of contaminants, meaning that additional stages of process are required. The membranes are sensitive to pH, oxidizers, organics, algae, and contaminants [3]. An important factor to consider is that RO has technological limitations which are especially important for the aspect of this thesis. The Red Sea is characterized by high temperature, salinity, turbidity, and marine life, all of which are likely to cause severe problems for RO based desalination systems [15].

1.2.2.5. Membrane distillation

In this system, which is a combination of membrane and thermal process, seawater is heated by solar energy and flows along a membrane. The membrane is porous and hydrophobic and only allows a passage of vapours. On the other side of a membrane, a cold seawater causes the condensation of fresh water which is then collected as the distillate. The separation is a result of vapour pressure difference on two sides of the membrane. The process can work in four main configurations: direct contact, air gap, sweeping gas or vacuum, depending on the type of contact on the cold side of the membrane. On the hot side there is always direct contact with the

membrane [11]. The configurations influence the heat and mass transfer of the process and can be selected according to the situation at hand.

There are many advantages to MD, such as high purity distillate, ability to work with lower temperatures than other methods and lower pressure, lack of need for expensive chemical pre-treatment and overall being a rather simple process. On the disadvantages side, quite low permeate flux, possible fouling and wetting phenomenon of the applied membrane, high membrane cost and overall high energy consumptions when compared to other methods can be observed [12] [9]. The method presents some potential, but still requires development and research to be able to compete with more mature methods.

1.2.2.6. Other membrane

Other membrane processes include electrodialysis or forward osmosis. Electrodialysis is based on removal of salts from seawater with the use of cation and anion exchange members by applying DC polarity across them [11]. Due to the direct current requirement, this system is generally used with photovoltaics systems rather than concentrated solar energy. It is not recommended for large scale seawater desalination due to high costs of ion exchange membranes, electrodes, and decreased lifetime of parts, especially when working with high salinity water [12]. Forward osmosis is a relatively new process which is based mainly on osmotic pressure difference. Use of draw solution which poses a high osmotic coefficient is required [9]. It carries advantages, such as lower energy consumption compared to RO, high salt rejection and simple equipment. Nonetheless, the process is only currently being investigated and in development stage, one of the problems being a difficulty in developing proper membranes [4].

1.2.3. Selection of the system

The majority of the described technologies are currently operating in different places around the world. They all carry some advantages and disadvantages. An important factor to consider when choosing the proper system is the location of the plant, as it allows to reject some options and emphasise the merits of others.

Regarding the concentrated solar energy, the main solutions are dish paraboloid concentrator, trough paraboloid concentrator, Fresnel lens and solar tower. The first option is the oldest one, but today not common and replaced by other, more efficient, solutions, so it can be ruled out. Fresnel lens carries interesting advantages but provides much lower optical efficiency and lacks large-scale applications. Of the remaining two both are well-developed and overall valuable solutions. The main disadvantages of solar tower are large area requirement and complex asynchronous two-dimensional tracking. The problems with paraboloid trough are high wind resistance and a potential decrease of efficiency due to dust accumulation. In this thesis, the location of the analysed CSP desalination station is Saudi Arabia. Since in that region sandstorms and soiling occur and there is no problem with area availability (due to presence of large desert areas), solar tower is the superior solution. Storage system is also included to allow for continuous operation of the desalination plant.

On the desalination side, the technologies still in development are ruled out, leaving multi-stage flash, multi-effect distillation and reverse osmosis. Out of the first two, multi-effect distillation is superior due to lower energy consumption, lower top brine temperature and better coupling with solar energy. Reverse osmosis is

currently the leading technology for desalination. The energy consumption is lower than in thermal methods, but mechanical energy or electricity is required to run the process, making the overall system more complex. In the considered location the source of seawater is the Red Sea. Its properties – high salinity, high temperature and high turbidity – may lead to severe problems when using reverse osmosis. As a result of this comparison, the most advantageous technology for the system can be concluded to be solar tower with storage coupled with multi-effect distillation. More thorough description of the system will be presented in the next chapter.

Table 1 - Advantages and disadvantages of selected technologies

Method	Advantages	Disadvantages
Concentrated solar energy		
Dish paraboloid	Very mature technology Easy installation Low wind resistance Optical efficiency up to 95% [16]	High capital and operation cost Complex HTF collection (usually coupled with Stirling engine) Reliability problems
Trough paraboloid	Very mature technology Dominant technology One-dimensional tracking Optical efficiency about 77% [17]	Prone to dust accumulation Decreased reflective properties High wind resistance
Fresnel lens	Low wind resistance Low cost of mirrors	No large-scale application Still developing Optical efficiency about 58% [18]
Solar tower	Mature technology High concentration ratio Optical efficiency about 76% [4]	Large area requirement Asynchronous two-dimensional tracking
Desalination		
Multi-stage flash	Second most dominant technology No pre-treatment of water required	High top brine temperature requirement Fouling and scaling problem Energy intensive (evaporation)
Multi-effect distillation	Lower top brine temperature No fouling and scaling problem No pre-treatment of water required	Energy intensive (evaporation)
Reverse osmosis	Dominant technology Lower energy requirement than thermal methods	High sensitivity of membranes Not recommended for Red Sea water

1.3.   Objective

The aim of this thesis is to perform a thermodynamic analysis of a concentrated solar energy desalination plant. Based on the performed review of technologies, solar tower with energy storage coupled with multi-effect distillation is considered. A thermodynamic cycle will be developed to simulate the operation and potential freshwater production. Each part of the system will be analysed, and then a model for the whole system will be prepared.

The location of plant considered in this thesis is Saudi Arabia and the Red Sea as the source of seawater. The Kingdom of Saudi Arabia makes an interesting location for such plant for several reasons. The region is characterised with desert climate, meaning that the temperatures are high and there is no precipitation; Saudi Arabia has one of the highest direct normal irradiation resources in the world. The energy consumption in the country is increasing, mainly due to the cooling demand and desalination of sea water [5] [19].

The temperature of water in the region is about 29°C with salinity of about 39.82 $\frac{g}{kg}$ [20]. The average daily total direct normal irradiance (DNI) in the region is about 5142 Wh/m^2 (measurements from 2013-2014) [21]. The design output power of desalination plant is 2 MW. The expected result from the analysis is mainly the amount of freshwater that can be produced. To achieve that, many other aspects are vital, such as the field of heliostats surrounding the tower and their capacity, and the storage system which allows to maintain a continuous operation of the desalination plant. The results of the analysis will be presented and discussed, along with possible improvements and changes to the system and potential future work.

1.4.   Methodology

As the aim of the thesis is to perform a thermodynamic analysis of a system, it is important to explain the methodology that will be followed along the process. After selecting the system, a model for each part will be developed based on available literature and then combined into one computational code. The model will be developed in Python [22] with packages NumPy [23], CoolProp [24], pandas [25] and Matplotlib [26]. The inputs to the model will be be either from design data, assumptions or based on analysed literature. Additionally, as solar energy is considered, weather data for the considered location will be used. The focus will be put on the thermal aspects of the system, therefore the calculations will mainly concern the heat transfer between the fluids and the heat losses to the environment. For the calculations, a steady state of system will be considered. However, for several parts of the system, the calculations will be performed on an hourly basis. The operation of the plant will be analysed over a period of one year.

2. Development of the model

2.1. Description of the system

As it was already described, the system consists of solar tower with storage system coupled with multi-effect distillation. Solar tower has two parts: heliostats and the central receiver.
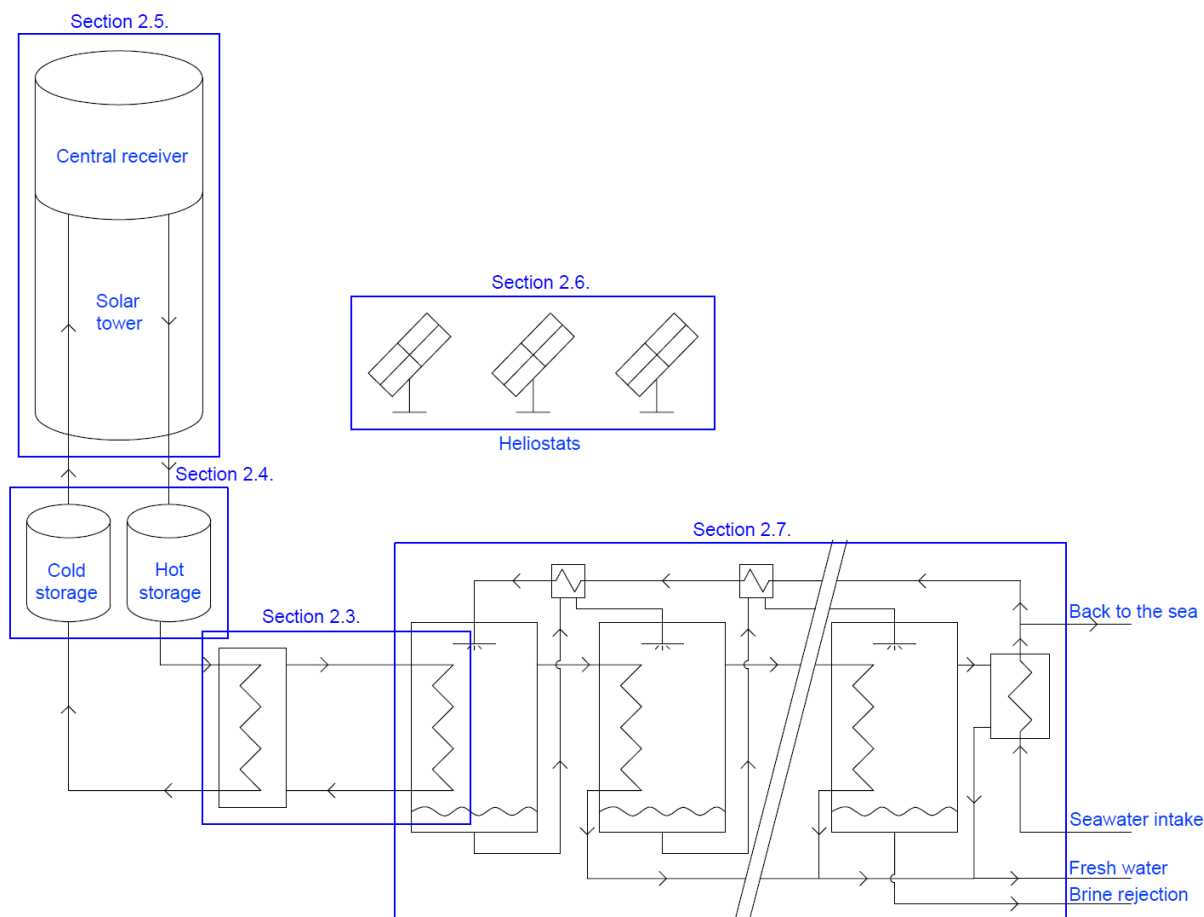
Figure 4 - Simplified scheme of the system

The heat transfer fluid used in the cycle is thermal oil Therminol 66. It can be operated in temperatures range of -3 to 345°C [27], which is within the requirement of this system. The operating temperatures range for molten salts (which are the most commonly used heat transfer fluids with solar towers) are very high and such high temperatures are not required for the process of desalination. Molten salts require trace heating to prevent excessive decrease of the temperature and crystallization [28]. Therminol can operate at temperatures even below the ambient temperatures in Saudi Arabia, so there is no risk of the occurrence of crystallization. With lower operating temperatures also the losses to the environment are decreased.

Regarding the central receiver, there are several options: multi-tube external receiver, multi-tube cavity receiver, volumetric receiver or particle receiver. The first two are far more investigated and developed [29], and are taken into consideration here. An external receiver consists of an array of panels with a certain number of tubes with heat transfer fluid. The panels are usually placed around the top of a cylindrical tower [30]. A cavity receiver implements a cavity in which a receiver is placed to reduce the heat losses. It is quite common in modern

CSP plants as due to the high fluid operating temperatures especially the radiative losses can be significant [30]. The advantage of external receivers is a simpler construction and possibility of application of 360° field of heliostats, as opposed to the cavity receivers, where the field is limited by the cavity shape. In this thesis an external receiver is considered. Since the heat transfer fluid is thermal oil and not molten salt, the operating temperatures are lower and thus losses to the environment are not as severe. The advantage is that 360° field of heliostats can be used and the receiver's design is overall simpler.

In multi-effect distillation the first effect is heated up by the energy from CSP. The required temperature is around 70 to 80°C, which allows to avoid scaling problems, but is high enough for the evaporation process to occur. MED has several possible configurations of operation – normal flow, contra flow and parallel flow [4]. Normal flow is characterised by the feed flowing from the first effect to the last one in sequence, with the temperature of each effect decreasing. In contra flow it is reversed – the feed flows from the last effect to the first one and the temperature is increasing. In parallel flow the feed flows to each effect independently and the brine does not flow to the next effect but is extracted. The contra flow is generally used for chemical processes and parallel flow for salt manufacturing. For producing fresh, drinkable water the normal feed is applied, and it will be the case in this analysis. The number of effects will be determined in the process. To maintain proper rate of heat transfer and production capacity of the plant, it is recommended to maintain the effective temperature difference between effects not lower than 5-7°C [4], so that rule will be followed in estimation of the number of effects.

To maintain the temperature of heating fluid for the first effect, an additional cycle is implemented. It consists of a heat exchanger and connection to the first effect. The working fluid is water. The heat exchanger heats up the water using the thermal oil as hot fluid.

The storage system consists of two tanks – one with hot fluid and one with cold fluid. The volume of the tanks will be calculated in the model. The tanks are insulated to decrease the heat exchange with the environment.

In the case of this system, the power output of the desalination station is known (2 MW). As a result, to calculate the requirements of the heliostat field, the calculations must be made from the last element (heating water cycle) back to the receiver to account for all losses in the system which need to be covered to deliver 2 MW of power to the desalination plant. Once the model for heating water cycle, storage and central receiver is developed, the requirements for the field of heliostats are known and their model can be implemented. As a last step, the model of multi-effect distillation will be developed.

2.2. General heat loss model

Heat losses are calculated several times, in different parts of the system. To simplify the description, a general heat loss model with required equations is presented here based on [31] and will be referred to later.

Rate of heat transfer $\dot{Q}$ is calculated as the temperature difference between two points ΔT divided by thermal resistance R between them.

$$\dot{Q} = \frac{\Delta T}{R} \tag{1}$$

Since the rate of heat transfer is constant in steady state, any two points in selected cross-section can be chosen. Thermal resistance is the sum of convective resistances R_h and conductive resistances R_c between the two points.

$$R_h = \frac{1}{h \cdot A} \tag{2}$$

$$R_c = \frac{\delta}{k \cdot A} \tag{3}$$

where h is the heat transfer coefficient, A is the area of heat transfer, δ is the thickness of the wall and k is the thermal conductivity of the material. For tubes, a different formula for conductive resistance is used:

$$R_c = \frac{\ln\dfrac{D_o}{D_i}}{2 \cdot \pi \cdot k \cdot L} \tag{4}$$

where D_o and D_i are outer and inner diameter of the tube and L is length of the tube. In this thesis most calculations are for tubes. In Figure 5 a sample cross-section of a tube is presented, with characteristic properties.
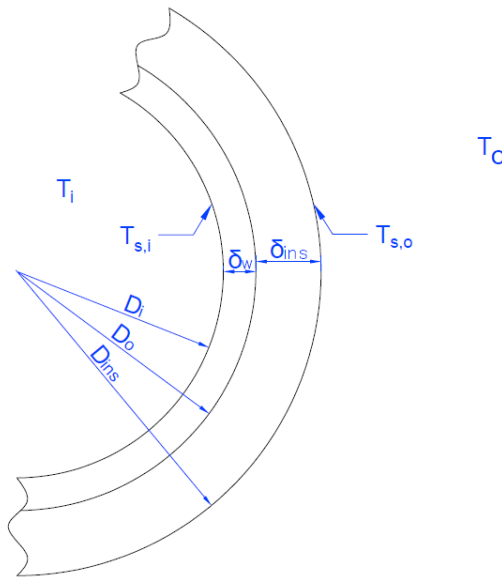

Figure 5 - Sample cross-section of a tube

Subscript i denotes the inner side, o the outer side, s a point on the surface, ins the insulation layer (which is often applied to reduce the heat losses) and w the wall.

Convective heat transfer coefficient is calculated from a Nusselt number Nu formula:

$$Nu = \frac{h \cdot L_c}{k} \tag{5}$$

$$h = \frac{Nu \cdot k}{L_c} \tag{6}$$

where L_c is a characteristic dimension which varies depending on the geometry and will be appointed properly in the subsequent parts. For forced convection as the mode of heat transfer, a correlation for Nusselt number is depending on the geometry and Reynolds number Re and will also be appointed properly depending on the studied case. Reynolds number is calculated based on velocity of the flow w, characteristic dimension, density ρ and dynamic viscosity μ. Velocity is calculated with mass flow rate of the fluid $\dot{m}$, fluid density and cross-section area of the flow A_f.

$$Re = \frac{w \cdot L_c \cdot \rho}{\mu} \tag{7}$$

$$w = \frac{\dot{m}}{A_f \cdot \rho} \tag{8}$$

For natural convection as the mode of heat transfer, a correlation for Nusselt number is chosen depending on the geometry and Rayleigh number Ra. Rayleigh number is a product of Grashof number Gr and Prandtl number Pr.

$$Ra = Gr \cdot Pr \tag{9}$$

$$Gr = \frac{g \cdot \beta \cdot (T_s - T) \cdot L_c^3 \cdot \rho}{\mu} \tag{10}$$

where g – gravitational acceleration equal to approximately $9.81 \frac{m}{s^2}$, β – coefficient of volumetric expansion. To decide which mode of convective heat transfer is dominant, a ratio of Grashof to squared Reynolds number is calculated, which is called Richardson number Ri. For values below 0.1 natural convection is negligible; for values above 10 forced convection can be neglected; for range between these two values both should be taken into account. In that case combined heat transfer coefficient is calculated.

$$Ri = \frac{Gr}{Re^2} \tag{11}$$

$$h = \left(h_{forced}^n + h_{natural}^n\right)^{1/n} \tag{12}$$

where $forced$ stands for forced convection, $natural$ for natural convection and n is a coefficient which depends on geometry, but generally 3 is used for a vertical surface and 4 for a horizontal one.

The radiative heat losses $\dot{Q}_{em}$ can be calculated with a simplified formula, if the surroundings are considered as a black body at ambient temperature:

$$\dot{Q}_{em} = \epsilon \cdot \sigma \cdot (T_s^4 - T_{amb}^4) \cdot A \tag{13}$$

where ϵ is emissivity of the surface, σ is Stefan-Boltzmann constant, equal to approximately $5.67 \cdot 10^{-8} \frac{W}{m^2 \cdot K}$ and T_{amb} is the ambient temperature.

2.3. Heating water cycle

Water in this cycle is heated up in a heat exchanger by a heat transfer fluid flowing from the hot storage tank and cooled down in the first effect of the desalination plant. The heat exchanger type is shell and tube, with heat transfer fluid on the shell side and water on the tube side.
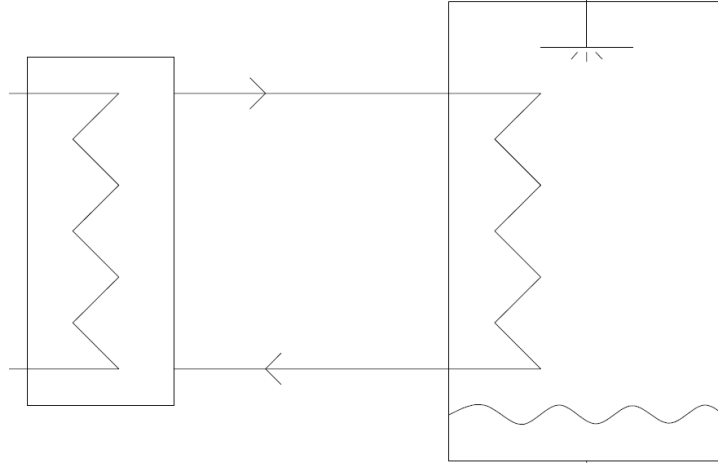
Figure 6 - Heating water cycle

First, the losses from the pipes are considered. Heat transfer coefficient of water is calculated using equation (6), with the characteristic dimension being the inner diameter of the pipe. Reynolds number is calculated using equation (7), also with the inner diameter as the characteristic dimension. For high accuracy, Gnielinski Nusselt number correlation [32] is used. Its additional advantage is a wide range of Reynolds number where it can be applied. The correlation includes friction factor f, which is obtained with first Petukhov equation [33].

$$Nu = \frac{\left(\frac{f}{8}\right) \cdot (Re - 1000) \cdot Pr}{1 + 12.7 \cdot \left(\frac{f}{8}\right)^{0.5} \cdot (Pr^{2/3} - 1)} \tag{14}$$

$$f = (0.79 \cdot \ln(Re) - 1.64)^{-2} \tag{15}$$

To calculate the heat transfer coefficient of air, properties of air should be obtained for average temperature between the outer surface of the insulation layer and ambient temperature of air. Since the surface temperature is not known at this point, the rate of heat transfer is assumed. Equation (1) is used with the temperature difference between the water and the surface temperature of the insulation layer and modified to calculate the latter.

$$\dot{Q} = \frac{T_{water} - T_{ins,s}}{R_{h,i} + R_{c,w} + R_{c,ins}} \tag{16}$$

$$T_{ins,s} = T_{water} - \dot{Q} \cdot \left(R_{h,i} + R_{c,w} + R_{c,ins}\right) \tag{17}$$

As the outer side of the pipe is considered here, it is subjected to both forced convection resulting from the wind and natural convection. Reynolds number is obtained with equation (7) to be used in forced convection calculations and Raileigh number with equations (9)-(10) for natural convection, using the outer diameter of the insulated pipe as characteristic length. Based on Richardson number obtained from equation (11) the dominant mode of heat transfer is assessed, and the heat transfer coefficient is calculated with equation (6). For forced convection, Nusselt correlation for flow over a cylinder by Churchill and Bernstein [34] is used:

$$Nu = 0.3 + \frac{0.62 \cdot Re^{1/2} \cdot Pr^{1/3}}{\left(1 + \frac{(0.4/Pr)^2}{3}\right)^{1/4}} \cdot \left(1 + \left(\frac{Re}{282000}\right)^{5/8}\right)^{4/5} \tag{18}$$

For natural convection, Nusselt correlation for flow over a cylinder by Churchill and Chu [35] is applied:

$$Nu = \left(0.6 + \frac{0.387 \cdot Ra^{1/6}}{(1 + (0.559/Pr)^{9/16})^{8/27}}\right)^2 \tag{19}$$

If both modes of convection heat transfer need to be considered, equation (12) is applied to calculate the mixed heat transfer coefficient. With obtained heat transfer coefficient of air, the losses from the pipes with water $\dot{Q}_{water,loss}$ are calculated with equation (1) for temperature difference between the water and ambient temperature.

$$\dot{Q}_{water,loss} = \frac{T_{water} - T_{amb}}{R_{h,i} + R_{c,w} + R_{c,ins} + R_{h,o}} \tag{20}$$

The calculated value is compared to the assumed one and the process is repeated until the difference is below 1%. Once the solution is converged, heat losses by convection and radiation can be calculated with equations (16) and (13), respectively. The process is then repeated for the cold pipe and all the losses are summed up.

For the heat exchanger part, first the heat transfer coefficient of the heat transfer fluid needs to be calculated. It is obtained using a correlation for Nusselt number for shell and tube heat exchangers [36] applied to equation for heat transfer coefficient (6).

$$Nu = 0.0126 \cdot Re^{0.8762} \cdot Pr^{0.289} \tag{21}$$

The characteristic dimension for the Reynolds number is equivalent shell side diameter D_e. To obtain the velocity of the flow on the shell side, cross-flow area of the shell A_s needs to be calculated [36].

$$D_e = \frac{1.27}{D_o} \cdot (P_t^2 - 0.785 \cdot D_o^2) \tag{22}$$

$$A_s = \frac{D_{sh} \cdot (P_t - D_o) \cdot B}{P_t} \tag{23}$$

$$P_t = 1.25 \cdot D_o \tag{24}$$

where P_t is the tube pitch, D_o is the outer diameter of the tube, D_{sh} is the shell diameter and B is the baffle spacing, assumed to be a third of shell diameter [36].

Heat transfer coefficient for water is calculated from equation (6), based on the Nusselt correlation by Gnielinski (14) and Reynolds number (7), with characteristic dimension being the inner diameter of the tube. To apply the formula from equation (2), for the convective heat resistance of the heat transfer fluid, the area of heat transfer is required. The diameter of the tube is known, but the length is not. To obtain it, first the logarithmic temperature difference in the heat exchanger ΔT_{log} and the overall heat transfer coefficient based on the outer area U_o [36] need to be calculated.

$$\Delta T_{log} = \frac{\Delta T_{in} - \Delta T_{out}}{\ln \frac{\Delta T_{in}}{\Delta T_{out}}} \tag{25}$$

$$U_o = \left(\frac{1}{h_o} + \frac{d_o \cdot \ln\left(\frac{d_o}{d_i}\right)}{k_w} + \frac{d_o}{d_i} \cdot \frac{1}{h_i} \right)^{-1} \tag{26}$$

where ΔT_{in} and ΔT_{out} represent the temperature difference at the inlet and outlet of the heat exchanger, respectively. The formula for the rate of heat transfer can be presented using the overall heat transfer coefficient and the logarithmic temperature difference, and upon a proper transformation it allows to calculate the length of the tubes.

$$\dot{Q} = U_o \cdot A_o \cdot \Delta T_{\log} = U_o \cdot \pi \cdot d_o \cdot L \cdot \Delta T_{log} \tag{27}$$

$$L = \frac{\dot{Q}}{U_o \cdot \pi \cdot d_o \cdot \Delta T_{log}} \tag{28}$$

The length of the tubes must be divided by number of tubes no_{tube} to obtain the length of the shell of the heat exchanger. Now it can be applied to obtain the convective thermal resistance of the HTF to use in equation (26) and compare to the assumed value. The process is repeated until the difference between the assumed and calculated temperature of the tube surface is below 1%.

Now the HTC of the air needs to be obtained. The procedure is the same as for the water heating loop. The rate of heat transfer is assumed to calculate the outer surface temperature of the insulation with equations (16)-(17) and Nusselt number with equations (18)-(19). Forced, natural or mixed convection is considered depending on the Richardson number, and the rate of heat transfer is recalculated until the difference between the assumed and calculated value is below 1%. Now the convective heat losses $\dot{Q}_{hex,loss,h}$ can be obtained from equation (1) for temperature difference between the heat transfer fluid and the surroundings.

$$\dot{Q}_{hex,loss,h} = \frac{T_{htf} - T_{amb}}{R_{h,htf} + R_{c,w} + R_{c,ins} + R_{h,o}} \tag{29}$$

The radiative heat losses $\dot{Q}_{hex,loss,em}$ (13) are calculated; all losses $\dot{Q}_{hex,loss}$ are then summed up and the efficiency (32) of the heat exchanger η_{hex} can be obtained, along with the heating loop $\eta_{water,loop}$ and the entire water heating system efficiency η_{water}, which accounts for losses from the pipes between the heat exchanger and the desalination plant - and from the heat exchanger.

$$\eta_{hex} = 1 - \frac{\dot{Q}_{hex,loss}}{\dot{Q}_{hex,in}} \tag{30}$$

$$\eta_{water,loop} = 1 - \frac{\dot{Q}_{water,loss}}{\left(\dot{Q}_{hex,in} - \dot{Q}_{hex,loss} \right)} \tag{31}$$

$$\eta_{water} = \eta_{hex} \cdot \eta_{water,loop} \tag{32}$$

where $\dot{Q}_{hex,in}$ is the rate of heat transfer delivered to the heat exchanger from the heat transfer fluid.

2.4. Storage

The storage system consists of two cylindrical tanks – one with hot fluid and one with cold fluid. Heat transfer fluid flows from the central receiver to the hot tank, then to the heat exchanger for heating water cycle, then to

the cold tank and from there again to the central receiver. Since the procedure for calculations of losses is the same for the hot and the cold tank, it will only be presented once.

The heat losses are divided into three parts: losses through the bottom to the ground, losses through the top and losses through the walls. Additionally, the losses through the walls are divided into two parts depending on the level in the tank – either heat transfer fluid level, or air level. First, the losses through the bottom are considered. The model suggested by Suárez et al. [37] is applied. A correlation for the soil equivalent thermal resistance $R_{c,soil}$ is presented.

$$R_{c,soil} = C \cdot \left(\frac{r_{st}}{k_{soil}}\right)^b \tag{33}$$

where C and b are coefficients, equal 0.4 and 0.85, respectively, r_{st} is the radius of the storage tank. Heat transfer coefficient of the heat transfer fluid in tank is calculated using equation (6). Since the heat transfer fluid is stored in the tank, it is assumed to be stationary, therefore only natural convection is considered. For the Nusselt number, a correlation for horizontal plate was used.

$$Nu = C \cdot Ra^n \tag{34}$$

where C, n are coefficients depending on the geometry and Rayleigh number (9). The characteristic length in this case is a ratio of the area to the perimeter of the surface. Heat transfer coefficient of the heat transfer fluid is to be calculated based on properties at the average temperature between the storage and the base of the tank $T_{st,b}$. Since the latter is not known, it is assumed and later recalculated. Generally, below the storage tank a layer of insulation is placed, and below that two layers of concrete with a cooling pipe between them to avoid exceeding the maximum temperature of concrete $T_{st,max}$, assumed to be 90°C. The highest temperature of concrete occurs on the top of the first layer.
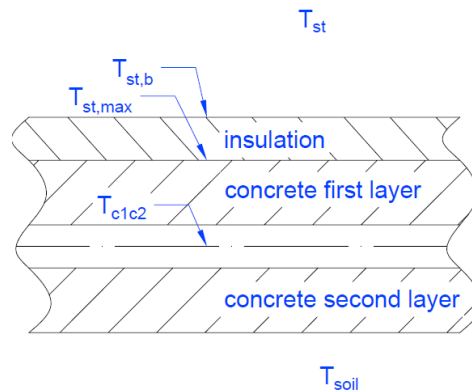
Figure 7 - Cross-section of layers below the hot storage tank

Heat losses through the bottom $\dot{Q}_{st,b}$ are calculated between the heat transfer fluid in the tank and the top of the first layer of concrete, using equation (1).

$$\dot{Q}_{st,b} = \frac{T_{st} - T_{st,max}}{R_{h,htf} + R_{c,ins}} \tag{35}$$

By modifying that equation to consider the temperature difference between the heat transfer fluid and the base of the tank, the temperature of the base can be calculated and compared to the assumed value. The process is repeated until the difference is no greater than 1%.

$$\dot{Q}_{st,b} = \frac{T_{st} - T_{st,b}}{R_{h,htf}} \tag{36}$$

$$T_{st,b} = T_{st} - \dot{Q}_{st,b} \cdot R_{h,htf} \tag{37}$$

where T_{st} is the storage temperature, $T_{st.b}$ is the temperature of the bottom surface. The losses through the bottom can now be divided into the ventilation requirements for the concrete and losses to the soil. First, the average temperature in the pipe (the average temperature of both concrete layers) T_{c1c2} needs to be obtained. It is calculated by modifying equation (1), for the temperature difference between the pipe and the maximum temperature of concrete.

$$\dot{Q}_{st,b} = \frac{T_{st,max} - T_{c1c2}}{R_{c,conc}} \tag{38}$$

$$T_{c1c2} = T_{st,max} - \dot{Q}_{st,b} \cdot R_{c,conc} \tag{39}$$

where conductive resistance $R_{c.conc}$ is that of the concrete. The temperature of the first layer of concrete is calculated as the average between the maximum temperature (at the top of the first layer) and the temperature of the pipe. The losses through the soil are calculated with equation (1) and temperature difference between the pipe and soil.

$$\dot{Q}_{soil} = \frac{T_{c1c2} - T_{soil}}{R_{c,conc} + R_{c,soil}} \tag{40}$$

where soil resistance is calculated using equation (33). The temperature of the soil is affected by many factors, mainly properties of the ground, ambient temperature, and depth. As the soil temperature can change even hourly with varying ambient temperature, to avoid the complexity of these calculations, a fixed value of 10°C is applied for this model [37]. Now, the ventilation requirements $\dot{Q}_{vent}$ are calculated as the difference between the losses though the bottom and losses to the soil.

$$\dot{Q}_{vent} = \dot{Q}_{st,b} - \dot{Q}_{soil} \tag{41}$$

For the top losses, heat transfer coefficient of air on the outside and the inside (it is assumed that the tank is never completely full) needs to be calculated. It is assumed that natural convection is the dominant mode of transfer on the inside, as the fluid is stored. For the outside, both modes of convection are considered and following the Richardson number (11) the heat transfer coefficient can be obtained. The Nusselt number coefficient for flow over flat plate is applied [31]:

$$Nu = 0.664 \cdot Re^{0.5} \cdot Pr^{1/3} \tag{42}$$

To calculate the heat transfer coefficients, fluid parameters need to be obtained for the average temperature between the surface and the bulk temperature of the fluid. Since neither of the surface temperatures is known,
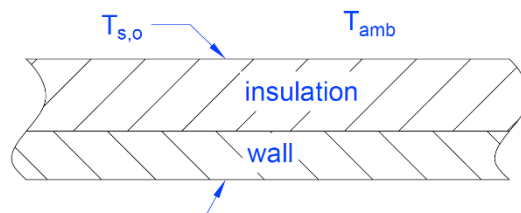

Figure 8 - Cross-section of layers on top of the hot storage tank

18

for this part the heat transfer coefficients are assumed and recalculated. The layers on the top along with the nomenclature are presented in Figure 8.

The surface temperatures $T_{s,i}$ and $T_{s,o}$ are calculated by properly modifying the heat transfer rate equation (1).

$$\dot{Q}_{top} = \frac{T_{st} - T_{amb}}{R_{h,i} + R_{c,w} + R_{c,ins} + R_{total,o}} \tag{43}$$

$$\dot{Q}_{top} = \frac{T_{st} - T_{s,o}}{R_{h,i} + R_{c,w} + R_{c,ins}} \tag{44}$$

$$T_{s,o} = T_{st} - \dot{Q}_{top} \cdot (R_{h,i} + R_{c,w} + R_{c,ins}) \tag{45}$$

$$\dot{Q}_{top} = \frac{T_{s,i} - T_{amb}}{R_{c,w} + R_{c,ins} + R_{h,o}} \tag{46}$$

$$T_{s,i} = T_{amb} + \dot{Q}_{top} \cdot (R_{c,w} + R_{c,ins} + R_{h,o}) \tag{47}$$

where $R_{total,o}$ stands for total thermal resistance on the outer side. To account for the radiative losses, radiative heat transfer coefficient $h_{em,o}$ is calculated [31] and included in total thermal resistance on the outer side. It is obtained by applying two different formulas for radiative heat transfer from the surface. The one in equation (48) is the same as in equation (13). The formula from equation (49) is a simplified formula including radiative heat transfer coefficient [38].

$$\dot{Q}_{top,em} = \epsilon \cdot \sigma \cdot \left(T_{s,o}^4 - T_{amb}^4\right) \cdot A_{st,o} \tag{48}$$

$$\dot{Q}_{top,em} = h_{em,o} \cdot A_{st,o} \cdot \left(T_{s,o} - T_{amb}\right) \tag{49}$$

$$R_{total,o} = \frac{1}{\left(h_{em,o} + h_{h,o}\right) \cdot A_{st,o}} \tag{50}$$

With the inner and outer surface temperatures, the average temperatures for the fluid parameters can be calculated and the heat transfer coefficients can be obtained using equation (6). The correlation for Nusselt number is the same as in equation (34) – for a vertical plate. Obtained heat transfer coefficients are compared to assumed values and the process is repeated until the difference is below 1%. The losses through the top $\dot{Q}_{st,top}$ are already obtained from this process.

Finally, the losses through the walls are calculated. Those losses are divided into two parts: the heat transfer fluid level and the air level. The outer surface temperatures may be different on these two levels which is why they should be separated. The process is very similar to the top losses. For calculation of the heat transfer coefficient on the inside of the tank, a different formula for Nusselt number is applied. It is a formula for vertical plates, but it is also applicable to vertical cylinders and it can be applied over the entire range of Rayleigh number. The characteristic dimension is in this case the height of the fluid level in the tank.

$$Nu = \left(0.825 + \frac{0.387 \cdot Ra^{1/6}}{\left(1 + \left(\frac{0.492}{Pr}\right)^{9/16}\right)^{8/27}} \right)^2 \tag{51}$$

For the outside of the tank, wind velocity is considered. Richardson number (11) is calculated based on Reynolds (7) and Grashof (10), with the characteristic dimension being the diameter of the tank and the height of the fluid

in the tank (either HTF or air), respectively, and either only one mode of convective heat transfer is considered (natural or forced), or both. For natural convection, Nusselt number correlation for a vertical cylinder is used (51); for forced convection, formula from equation (18) is applied (for flow over a cylinder). Once again, the heat transfer coefficients are first assumed and then recalculated, until the difference is below 1%. The process is the same for the heat transfer fluid level and the air level in the tank.

The losses from the top, bottom and wall (for both fluid levels) are summed up to total loss from storage system $\dot{Q}_{loss,st}$. Since in the storage tank the losses are dependent on the level to which the tank is filled – as it changes the 'air level' and 'fluid level' and corresponding heat transfer coefficients as well as the amount of energy stored in the tank Q_{st}, the losses need to be calculated for every hour of operation.

$$Q_{st} = H_{st,htf} \cdot A_{st,b} \cdot \rho_{htf} \cdot I_{htf} \tag{52}$$

$$\eta_{st} = \frac{Q_{st} - \dot{Q}_{loss,st} \cdot 3600s}{Q_{st}}$$

where I_{htf} is the specific enthalpy $\left[\frac{J}{kg}\right]$ of heat transfer fluid. As the losses are in W, they are multiplied by 1 hour (3600s) to obtain the amount of energy lost over one hour. The exact procedure of hourly calculation of losses from the system is presented in section 2.8.

2.4.1. Validation of the model

The model of the losses through the bottom was implemented in Python and it was verified by comparing the obtained results with results presented in Suárez et al. [37]. The conditions from the paper, presented in Table 2, were recreated and the simulation performed. The conditions below the double line were not given in paper but assumed and only influenced the second part of the validation, for losses through the walls and the top. Figure 9 compares the results from the paper and from the implemented model. As it can be observed, the results from the implemented model are very close to those from the paper (the highest difference is about 3%), therefore it can be stated that the model was implemented correctly. $\dot{q}_{st,b}$ stands for heat flux, which is obtained by dividing the rate of heat transfer by surface area.

$$\dot{q}_{st,b} = \frac{\dot{Q}_{st,b}}{A_{st,b}} \tag{53}$$

Table 2 - Conditions for validation of the storage tank model

Parameter	Value
Storage temperature, °C	386
Tank diameter, m	38.5
Concrete layer thickness, m	0.45
Soil temperature, °C	10
Soil conductivity, $\frac{W}{m^2 \cdot K}$	2
Concrete max temperature, °C	90
Insulation conductivity, $\frac{W}{m^2 \cdot K}$	$1.7 \cdot (1 + 0.005 \cdot T_{ins})$
Heat transfer fluid	Molten salt
Tank height, m	20
Tank fill level, %	90
Insulation thickness, m	0.5
Wind speed, m/s	5
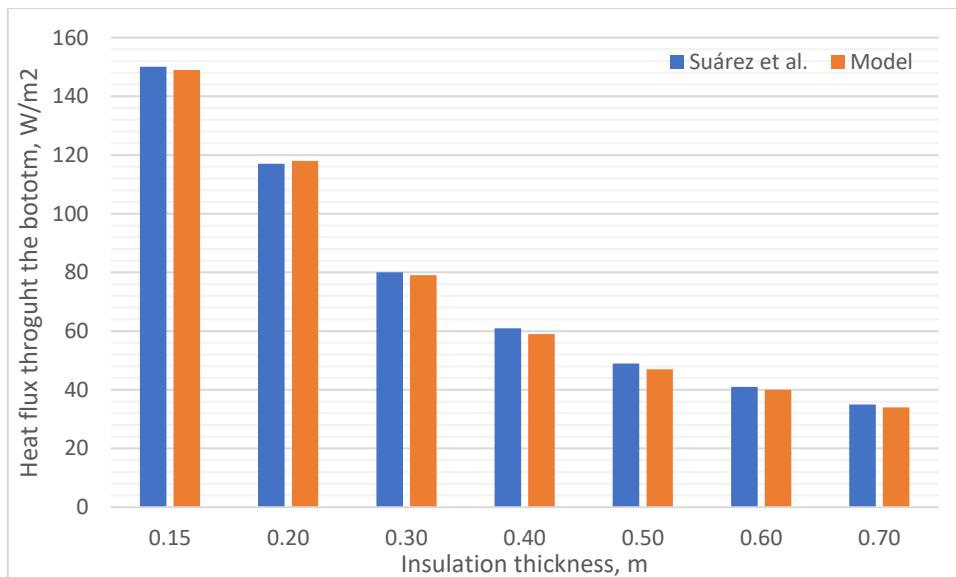
Figure 9 - Validation of the storage tank model [37]

In the analysed paper, only the losses through the bottom of tank are presented. Since the model for losses through the side walls and the top is general and very dependent on the conditions of the system, there is no possibility to directly validate it. A general comparison of the values of the heat transfer coefficients is performed based on typical values [31] [39] to see if they are within the expected ranges and if any major mistakes can be

noticed. The conditions for the test are as presented in Table 2. In the applied model, the HTC of the heat transfer fluid inside the tank (subjected only to natural convection) is 170 $\frac{W}{m^2 \cdot K}$, where the range of typical values is 10 $\frac{W}{m^2 \cdot K}$ – 1000 $\frac{W}{m^2 \cdot K}$, so it is within that range. For the air inside the tank, also subjected only to natural convection, it is about 3.5 $\frac{W}{m^2 \cdot K}$; the range is from 2 $\frac{W}{m^2 \cdot K}$ to 25 $\frac{W}{m^2 \cdot K}$. For air on the outside, subjected to mixed or forced convection, the value of the HTC is about 10 $\frac{W}{m^2 \cdot K}$. The typical range is from 10 $\frac{W}{m^2 \cdot K}$ to 250 $\frac{W}{m^2 \cdot K}$, so the obtained result is on the lower limit, but within that range. The values of HTC for the top part, namely air on the inside, is around 1 $\frac{W}{m^2 \cdot K}$. This is a little below the range; however, only a simple correlation for Nusselt number is available for that geometry and thus it may be less accurate. For the outside air on the top of the storage tank, it is about 12 $\frac{W}{m^2 \cdot K}$, so once again within the expected range. As all the obtained heat transfer coefficients are either within the typical range or close, it can be expected that no major mistakes were made in their estimation.

2.5. Central receiver

As it was already mentioned, the type of considered central receiver is external. The receiver converts concentrated solar energy into thermal energy, so its efficiency is particularly important for the entire system. A thermal model suggested by Li et al [40] is applied, with certain formulas from Çengel [31]. It is a steady-state model designed mainly for cavity receivers, but it is also applicable to external receivers. Regarding the geometry, an external receiver is usually of cylindric shape, with panels mounted around the cylinder. Each panel consists of a certain number of tubes. To simplify the inputs for the model, the area of the receiver is calculated based on design capacity $\dot{Q}_{re,in}$ and design peak heat flux $\dot{q}_{re,in}$. To account for factors such as spillage and the changes of heat flux throughout the operation of the receiver, it is recommended that the actual area of the receiver A_{re} is 4.5 times higher than the calculated one $A_{re,calc}$ [41].

$$A_{re,calc} = \frac{\dot{Q}_{re,in}}{\dot{q}_{re,in}} \tag{54}$$

$$A_{re} = 4.5 \cdot A_{re,calc} \tag{55}$$

Generally, for this type of receiver the ratio of height to diameter should be between 1 and 2 [42]. For this analysis, it is taken as 1.5, and it allows to calculate the height of the receiver H_{re} and its diameter D_{re}.

$$A_{re} = \pi \cdot D_{re} \cdot H_{re} \cdot \frac{\pi}{2} \tag{56}$$

$$D_{re} = \sqrt{\frac{A_{re}}{\pi \cdot 1.5 \cdot \frac{\pi}{2}}} \tag{57}$$

$$H_{re} = 1.5 \cdot D_{re} \tag{58}$$

As the wall of the receiver is not flat but it is covered by the tubes as shown in Figure 10, a factor of $\frac{\pi}{2}$ is added to the area in equation (56) to account for the curvature of the tubes on the outer surface of the receiver [42].
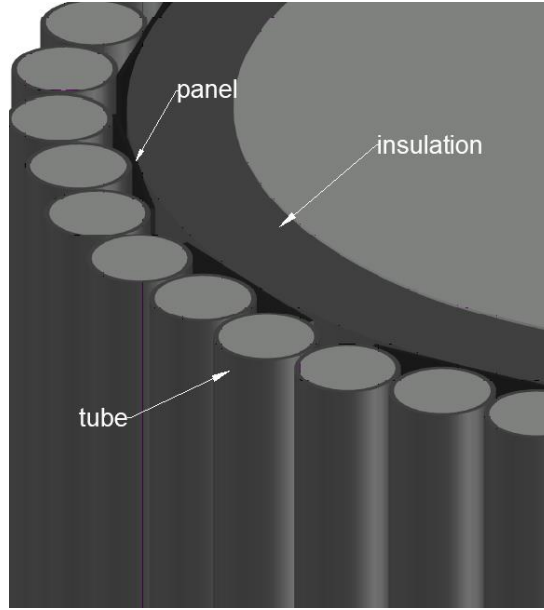
Figure 10 - Scheme of a portion of an external receiver

The output of the model is the efficiency of the receiver η_{re} and the energy absorbed by the heat transfer fluid $\dot{Q}_{re,abs}$. The calculated losses account for the emissive losses $\dot{Q}_{re,em}$, the reflective losses $\dot{Q}_{re,ref}$, the convective losses $\dot{Q}_{re,h}$ and the conductive losses $\dot{Q}_{re,c}$. At this stage, the total losses need to be assumed, as 10% of incident energy $\dot{Q}_{re,in}$; that value is later replaced by a calculated one. The incident energy comes from the heliostat field. First, the total energy balance equation is applied.

$$\dot{Q}_{re,in} = \dot{Q}_{re,total} + \dot{Q}_{re,abs} \tag{59}$$

$$\dot{Q}_{re,abs} = \dot{Q}_{re,in} - \dot{Q}_{re,total} \tag{60}$$

where $\dot{Q}_{re,total}$ is the sum of all the losses. To calculate the subsequent losses, the temperature of the receiver surface needs to be obtained. Equation (1) was used for the temperature difference between the temperature of the surface of the receiver and of the heat transfer fluid. For the heat transfer fluid temperature, it was assumed that the temperature is constant throughout the receiver and equal to the average temperature between the inlet and the outlet, thus the surface temperature was also assumed to not change along the tubes.

$$\dot{Q}_{re,in} = \frac{T_{re,sur} - T_{htf}}{R_{h,htf} + R_{c,w}} \tag{61}$$

$$T_{re,sur} = \dot{Q}_{re,in} \cdot \left(R_{h,htf} + R_{c,w} \right) + T_{htf} \tag{62}$$

The area for the convective heat resistance is the inner area of all tubes. The heat transfer coefficient is obtained from equation (6); for the Nusselt number, the correlation by Gnielinski is applied (14). With the temperature of the surface of the receiver, subsequent losses can be calculated.

2.5.1. The radiative losses

For the radiative heat losses, it is assumed that the temperature of the receiver surface is uniform and that there is no heat transfer between different parts of receiver. Although in reality some heat is lost by the tubes in the direction of other tubes, as a result some is also absorbed. However, since incident heat flux from the heliostats

on any two adjoint pipes is very similar, it can be assumed that heat loss and absorption by a pipe will cancel out. The radiative losses were calculated considering the emissivity of the receiver ϵ_{re}.

$$\dot{Q}_{re,em} = \epsilon_{re} \cdot \sigma \cdot \left(T_{re,sur}^4 - T_{amb}^4 \right) \cdot A_{re} \tag{63}$$

2.5.2. The reflective losses

To avoid overly complex calculations, it is assumed that the surface reflectivity does not change with the change of the receiver temperature. Therefore, the reflective losses $\dot{Q}_{re,ref}$ are calculated using constant surface reflectivity ref_{re}.

$$\dot{Q}_{re,ref} = \dot{Q}_{re,in} \cdot ref_{re} \tag{64}$$

2.5.3. The convective losses

For the convective heat losses, Grashof number (10), with characteristic dimension being the height of the receiver, and Reynolds number (7), with characteristic dimension being the diameter of the tower, are calculated. Based on the Richardson number (11) either only one mode of convective heat transfer is considered or both. The Nusselt number correlations for flow over a cylinder are applied (the receiver, consisting of a series of pipes, is considered as cylinder) from equations (18)-(19) and the heat transfer coefficient of air h_{air} is calculated (6). Should both modes of convective heat transfer be considered, equation (12) is applied to obtained mixed heat transfer coefficient. The convective heat losses are calculated with equation (1), for temperature difference between the receiver surface and ambient temperature.

$$\dot{Q}_{re,h} = \frac{T_{re,sur} - T_{amb}}{R_{h,air}} \tag{65}$$

2.5.4. The conductive losses

The conductive losses have the smallest share of all heat losses for the receiver; they compose of losses to the insulation layer behind the tubes and to the supports. Only losses to the insulation are considered in this model, as they are much greater than the latter one. Since the insulation wall temperature is not known at this point, and is required to calculate the heat transfer coefficient of air, it is assumed and then corrected. Heat transfer coefficient is obtained using the equation (51) as the correlation for the Nusselt number (for natural convection over a vertical plate). Since this part is inside the cylinder and not subjected to wind, only natural convection is considered. Modified equation (1) is applied to calculate the losses and to recalculate the temperature on the surface of the insulation layer. The temperature difference between the surface of the insulation layer and the surface of the receiver and between the ambient temperature and the temperature of the surface of the insulation layer is used.

$$\dot{Q}_{re,c} = \frac{T_{re,sur} - T_{ins}}{R_c} \tag{66}$$

$$\dot{Q}_{re,c} = \frac{T_{ins} - T_{amb}}{R_h} \tag{67}$$

$$T_{ins} = \dot{Q}_{re,cond} \cdot R_h + T_{amb} \tag{68}$$

The process is repeated until the difference between the assumed value and calculated value of the temperature is below 1%.

All the losses – emissive, reflective, convective and conductive – are summed up and the efficiency of the tower can be calculated same as it was done with equation (32). The efficiency of the tower is dependent on the incident energy from the heliostat field. For better accuracy, it will be calculated for every hour to account for changing weather conditions and resulting different incident energy.

2.5.5. Validation of the model

The model was implemented in Python and the conditions from Li et al. [40] were recreated. The conditions are presented in Table 3 and the comparison of the results is given in Figure 11. It is worth to notice that a view factor appears here. As the model presented in the paper was tested with a cavity receiver, the view factor had to be considered in the radiative losses as they are lower for a cavity receiver due to its shape.

Table 3 - Conditions for validation of the central receiver model

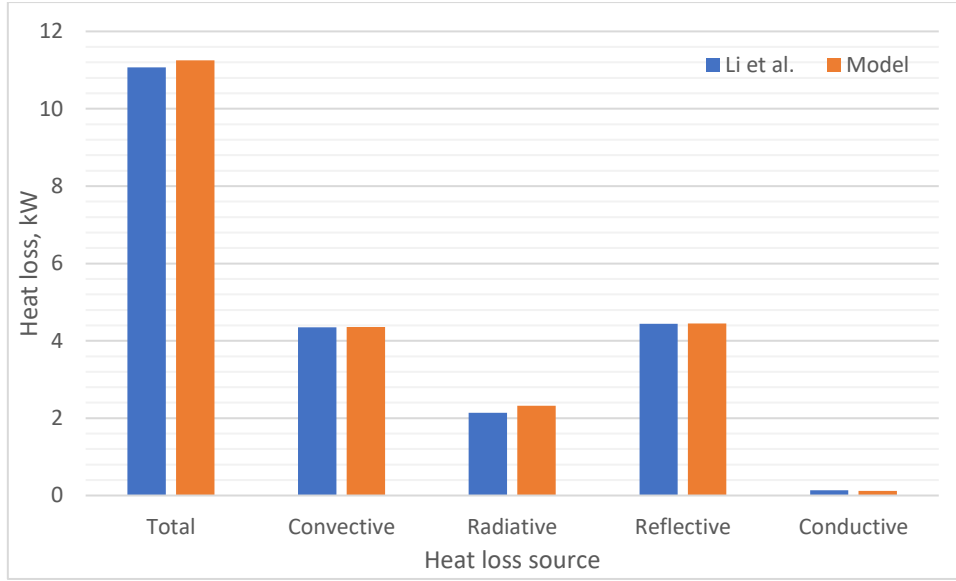| Parameter	Value
Hot HTF temperature, °C	560
Cold HTF temperature, °C	290
Absorbed energy, kW	100
Receiver area, m^2	0.2895
Tube diameter, m	0.019
Tube thickness, m	0.00165
Tube conductivity, $\frac{W}{m \cdot K}$	19.7
Emissivity, -	0.8
Reflectivity, -	0.04
Insulation layer thickness, m	0.07
Heat transfer fluid	Molten salt
View factor, -	0.8

Figure 11 - Validation of the central receiver model [40]

As it can be observed, the results of the implemented model are very close to that from the paper. The greatest difference is in the radiative losses. At some stages different (more complex) formulas were applied than those suggested in paper, most likely resulting in different value of the surface temperature and reflecting on the emissive losses. Overall, the implementation of the model can be assessed as correct.

2.6. Heliostats

The model of heliostats is developed mainly based on [43]. The instantaneous efficiency of a heliostat field η_{he} can be obtained by multiplying several loss factors [44]:

$$\eta_{he} = \eta_{he,\cos} \cdot \eta_{he,att} \cdot \eta_{he,ref} \cdot \eta_{he,sb} \cdot \eta_{he,spill} \tag{69}$$

where $\eta_{he,cos}$ accounts for cosine loss, $\eta_{he,att}$ for atmospheric attenuation loss, $\eta_{he,ref}$ for heliostat reflectivity, $\eta_{he,sb}$ for shadowing and blocking loss and $\eta_{he,spill}$ for spillage loss. For a heliostat field, the crucial factor is the location of heliostats around the tower, as some losses are location dependent. The majority of existing solar tower plants use a radial staggered configuration, where heliostats are placed along circular arcs of increasing radius called rows and are staggered in rows to minimise the shadowing and blocking loss [43], and the same configuration is applied in this model.
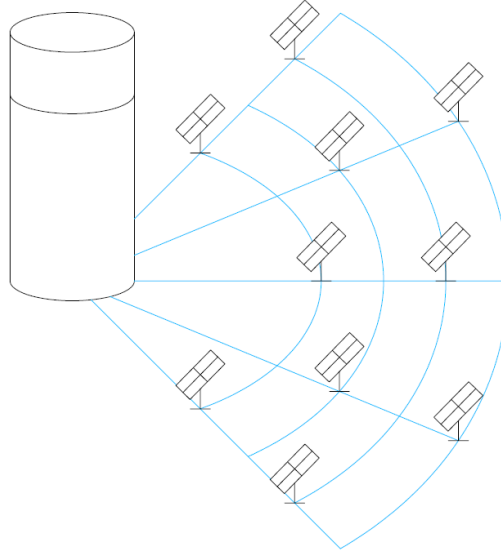
Figure 12 - Radial staggered heliostat field layout scheme

To consider the position dependent losses, first a field for calculations is created, called from now theoretical heliostat field, with solar tower in the middle (position 0,0), and extending 10 units to each side. In order to increase the range of application of the model, instead of units of distance a non-dimensional ratio of distance to tower height is used – either $\frac{x}{H_{to}}$ or $\frac{y}{H_{to}}$. Each of the cells is divided into 4 parts in horizontal and in vertical direction, resulting in non-dimensional elemental length $\frac{d_x}{H_{to}}$ and width $\frac{d_y}{H_{to}}$ of 0.25. Each of the cells will be analysed as a potential location for heliostats considering subsequent losses.

2.6.1. Cosine loss

Cosine loss occurs as a result of the effective reflection area of the heliostat being reduced by the cosine of the sun's incident angle [43]. It is dependent on the location of the heliostat in the field and on time of day. First, several angles need to be calculated. Declination angle θ_{dec}, which is dependent on the day of the year day, hour angle θ_{hour} dependent on hour of the day $hour$, zenith angle θ_z dependent on latitude of the location lat and altitude angle θ_{alt} being a function of zenith angle.

$$\theta_{dec} = 23.45 \cdot \sin\left(\left(\frac{360}{365}\right) \cdot (284 + day)\right) \tag{70}$$

$$\theta_{hour} = 15 \cdot (hour - 12.5) \tag{71}$$

$$\theta_z = \arccos\big((cos(lat) \cdot cos(\theta_{dec}) \cdot cos(\theta_{hour})) + (sin(lat) \cdot sin(\theta_{dec}))\big) \tag{72}$$

$$\theta_{alt} = 90 - \theta_z \tag{73}$$

It is worth to notice that in equation (71) 12.5 is subtracted from the hour of the day rather than 12. This results in the cosine loss being calculate in mid hour rather than in full hour. The reason for that is that at hour 12, the hour angle would equal 0 and then could cause issues in calculations in the subsequent steps. As this half an hour change is applied throughout the entire day, it should not have a significant impact on the results, and allows to avoid additional problems in the calculations. Azimuth angle θ_{az} is obtained based on previously calculated parameters.

$$\theta_{az} = \arccos\left(\frac{sin(\theta_{dec}) \cdot cos(lat) - cos(\theta_{dec}) \cdot sin(lat) \cdot cos(\theta_{hour})}{cos(\theta_{alt})}\right) \quad (74)$$

An additional condition is introduced – for sine of hour angle above zero, azimuth angle is recalculated as $360 - \theta_{az}$; for nonpositive values of the sine it does not change.

Now the value of cosine angle $cos(\theta_{i,j})$ is calculated in two steps. As it was mentioned, it is dependent on the location j and time i. The location is defined by two parameters from the preciously created field - $\frac{x}{H_{to}}$ and $\frac{y}{H_{to}}$, whereas time is defined by the hour of the year.

$$cos(2\theta_{i,j}) = \frac{sin(\theta_{alt}) - \frac{x}{H_{to}} \cdot cos(\theta_{alt}) \cdot sin(\theta_{az}) - \frac{y}{H_{to}} \cdot cos(\theta_{alt}) \cdot cos(\theta_{az})}{\sqrt{1 + \left(\frac{x}{H_{to}}\right)^2 + \left(\frac{y}{H_{to}}\right)^2}} \quad (75)$$

$$cos(\theta_{i,j}) = \sqrt{\frac{1 + cos(2\theta_{i,j})}{2}} \quad (76)$$

The process is rather complex as it requires the calculation of cosine angle for every hour for every position in the field, however, it allows to analyse the entire field surrounding the tower and to find the preferred location of the heliostats.

2.6.2. Atmospheric attenuation loss

This loss occurs due to the atmospheric attenuation, which causes the decrease of radiation along its path [45]. This loss is location dependent, so it is calculated for every point j in the field. Two models are considered: for a clear day and for a hazy day. Since in the analysed region clear days are dominating, the following formula is applied.

$$\eta_{he,att,j} = 0.99326 - 0.1046 \cdot S_j + 0.017 \cdot S_j^2 - 0.002845 \cdot S_j^3 \quad (77)$$

where S_j is the slant height of the point j from the top of the tower, in kilometres.

$$S_j = \frac{\sqrt{x_j^2 + y_j^2 + H_{to}^2}}{1000} \quad (78)$$

The height of the tower H_{to} is not known at this point, and it will be determined and described later.

2.6.3. Reflectivity loss

Reflectivity efficiency $\eta_{he,ref}$ represents the quality of the reflective surface. It is based on the material of heliostat, but also on the degradation and the heliostat's cleanliness. Since the variation of the two latter parameters over time is difficult to establish, a constant value for this loss, equal to 0.88 [44], over the entire time is assumed.

2.6.4. Shadowing and blocking loss

The losses related to shadowing and blocking are the most complex ones to analyse. Around each heliostat a group of heliostats is considered and checked geometrically for shadowing and blocking influence on the analysed heliostat. The mirror outlines are projected onto the planes of the neighbouring mirrors and checked

for potential interference. Regarding the shading, the projection must follow the rays of the sun and their change over time [46]. This means that the loss is dependent not only on time and location in the field, but also position of surrounding heliostats. The method, called Monte Carlo Ray Tracing, is computationally expensive and not very practical in simple analyses. Certain methods which simplify the process have been developed, such as discretization of the heliostats for improvement of the process [47] or using the Graphic Processing Units to shorten the computation time [48]. However, the methods are still extremely complex and such high accuracy is not required for the analysis performed here.

In this thesis, a somewhat different approach is taken. In simplified cases, the shadowing and blocking loss may be neglected or assumed to be constant [47]. A value of the efficiency $\eta_{he,sb}$ is considered as 0.95 for yearly average and based on research of existing heliostat fields [49] [50]. However, neglecting these losses would suggest that heliostats can be placed directly next to one another. To account for gaps in the heliostat field layout, a parameter called packing density PD is calculated [43]. It is the local ratio of mirror area to land area, varying with radial distance from the solar tower $\frac{r}{H_{to}}$, developed based on existing heliostat field layouts. The radial distance from the solar tower is calculated based on the location in the analysed field.

$$\frac{r}{H_{to}} = \sqrt{\left(\frac{x}{H_{to}}\right)^2 + \left(\frac{y}{H_{to}}\right)^2} \tag{79}$$

The packing density is calculated with one of three formulas depending on the value of the radial distance for every cell in the theoretical heliostat field. The conditions and formulas are presented in Table 4.

Table 4 - Conditions and formulas for packing density

Condition	Formula	
$\frac{r}{H_{to}} < \frac{r}{H_{to\,min}}$	$PD = 0$	(80)
$\frac{r}{H_{to\,min}} \le \frac{r}{H_{to}} \le 2.8$	$PD = 0.492 - 0.0939 \cdot \frac{r}{H_{to}}$	(81)
$\frac{r}{H_{to}} > 2.8$	$PD = \dfrac{0.6}{\sqrt{\left(\frac{r}{H_{to}}\right)^2 - 1}}$	(82)

where $\frac{r}{H_{to\,min}}$ is the minimum radial distance from the tower, assumed to be half of the tower height. In the next sections, in the calculation of the solar energy collected from each cell, packing density will be used to account for gaps between heliostats.

2.6.5. Spillage loss

The spillage loss is also called the interception efficiency $\eta_{he,sp}$. It concerns the part of solar radiation reflected by the heliostats towards the central receiver which does not fall on the absorbing area [51]. The loss depends on the location of heliostats in the fields and shape and properties of the central receiver. The method of Monte Carlo Ray Tracing, similar to that from the shadowing and blocking loss, is currently often replaced by a new model, based on HFLCAL model, as it is easier and faster to use [52]. However, it is still complex. Based on the analysis presented in [53], the average spillage loss from the entire field of heliostats is about 1.2%. Given that

the value is very low, to make the model of the system simpler, the value of this loss is not calculated but assumed constant throughout the field.

2.6.6. Process description

With the types of losses and their method of calculations presented, now the steps of the process are described. The rated capacity P_{cap} is equal to the required capacity for the desalination plant P_D, in this case 2 MW, divided by the efficiency of subsequent parts of the system – the water heating cycle, the thermal storage, the central receiver and the field of heliostats. Since the values are required only for a preliminary estimate of required capacity, they do not need to be exact. Average values are used for the water heating cycle, thermal storage and central receiver based on performed calculations, and for heliostat a value of 60% from literature [54] is used.

$$P_{cap} = \frac{P_d}{\eta_{water} \cdot \eta_{st} \cdot \eta_{re} \cdot \eta_{he}} \tag{83}$$

Considering that the system is designed to use storage system, equivalent capacity $P_{eq,cap}$ needs to be calculated to account for the time of storage.

$$P_{eq,cap} = P_{cap} \cdot \frac{t_{oper} + t_{st}}{t_{oper}} \tag{84}$$

where t_{oper} is the average time of operation of the heliostat field per day and t_{st} is the average number of hours for which the thermal storage needs to account. Those times are calculated based on weather data and taken as averages from an entire year.

Now the main operation on the theoretical heliostat field around the central receiver begins. First, following the description, the cosine losses are calculated. Parameters from equations (70)-(74) are calculated for every hour of the year and then with equations (75)-(76) the value of cosine angle is obtained, for every hour of the year in each position of the created field. Then the total annual solar energy $e_{m,j}$ per mirror area is calculated by multiplying the cosine values by direct normal irradiation DNI in each hour and the values are summed over all hours for each location.

$$e_{m,j} = \sum_{i=0}^{8760} \left(DNI_i \cdot \cos(\theta_{i,j}) \right) \tag{85}$$

Considering that there exists some variation of DNI between morning and afternoon, the values of $e_{m,j}$ are not exactly symmetrical regarding to the north-south axis. However, in practical applications the heliostats surrounding the tower are placed symmetrically. To account for that, an average value of any two points symmetrical regarding to the north-south axis is used and applied in both points.

Following the shadowing and blocking loss description, the packing density is calculated for every point in the field. It is then multiplied by the obtained total annual solar energy to obtain the actual annual reflected energy per unit land area $e_{l,j}$.

$$e_{l,j} = PD_j \cdot e_{m,j} \tag{86}$$

With that value the outer solar field boundary needs to be defined to find a range in which heliostats should be placed. It is generally assumed to be not lower than 0.16 MWh/m^2, based on existing plants data [43]. For this

analysis, it is assumed as 0.20. This allows to find limit of the heliostat field, as with increasing distance from the tower this value is decreasing. In locations where the actual annual reflected energy per unit land area is below the assumed value, no heliostats are placed and therefore the reflected energy is set to zero. The remaining points in the field boundary are denoted as N_f.

The only remaining location dependent loss is the attenuation loss. To calculate it, the height of the tower must be known. It is obtained with an iterative process organised to find the required height of the tower for the capacity of the field. First, for each hour the value of $P_{i,a}$ needs to be calculated.

$$P_{i,a} = \eta_{he} \cdot \frac{d_x}{H_{to}} \cdot \frac{d_y}{H_{to}} \cdot \sum_{j=1}^{N_f} \left(DNI_i \cdot \cos(\theta_{i,j}) \cdot PD \cdot 1 \right) \qquad (87)$$

$$\eta_{he} = \eta_{he,ref} \cdot \eta_{he,sb} \cdot \eta_{he,sp} \qquad (88)$$

where $P_{i,a} \cdot H_{to}^2$ is the solar power collected for each hour, neglecting the attenuation losses, and η_{he} is the average efficiency of the heliostat field being the product of efficiencies of subsequent losses. The tower height must be such that the maximum collected solar power $P_{a,max}$ is very close to the design equivalent capacity. For the first iteration the height of the tower is calculated as follows:

$$H_{to} = \sqrt{\frac{P_{eq,cap}}{P_{a,max}}} \qquad (89)$$

Now with that height the non-dimensional slant height $S_{n,nd,j}$ for each point j is calculated, and then the actual slant height $S_{n,j}$.

$$S_{n,nd,j} = \frac{\sqrt{\left(\frac{x}{H_{to}}\right)^2 + \left(\frac{y}{H_{to}}\right)^2 + (1)^2}}{1000} \qquad (90)$$

$$S_{n,j} = S_{n,nd,j} \cdot H_{to} \qquad (91)$$

The attenuation model is applied from equation (77) is applied and now for each hour the solar power collected from the heliostat field P_i can be obtained.

$$P_i = \eta_{he} \cdot \left(\frac{d_x}{h_{to}}\right) \cdot \left(\frac{d_y}{h_{to}}\right) \cdot H_{to}^2 \cdot \sum_{j=1}^{N_f} \left(DNI_i \cdot \cos(\theta_{i,j}) \cdot PD \cdot \eta_{he,att,j} \right) \qquad (92)$$

From all those values the maximum is checked if it is below the equivalent design capacity. If it is, the height of the tower is increased by ΔH_{to}, assumed to be 5 metres, and process goes back to equation (91). If not, the height of the tower is decreased by ΔH_{to}, the value of ΔH_{to} is divided by 10, tower height is increased by the new increment and that new height is applied in equation (91). The process continues until the increment for tower height is below 0.1 metres.

2.6.7. Validation of the model

The described model was implemented in Python and the results were compared against those presented in Srilakshmi et al. [43]. Some parameters were not specified in the paper, so ideal recreation of the conditions was not possible. The conditions used for the comparison are presented Table 5.

Table 5 - Conditions for validation of the heliostat field model

Parameter	Value
Location	Jodhpur, India
Year (assumed)	2011
Thermal storage, hours	0
Outer solar field boundary, MWh/m^2	0.16
Power block efficiency, -	0.44

The location of the plant analysed in the paper is the region of Jodhpur, India, but exact position is not mentioned. Also, the year for which the analysis was performed is not given; for the simulation of the model the weather data for 2011 was used. Power block efficiency is present here as for the simulation in paper the heliostat field was used to generate electricity, not heat. The results of the annual electrical energy obtained for different design capacities is presented in Figure 13.
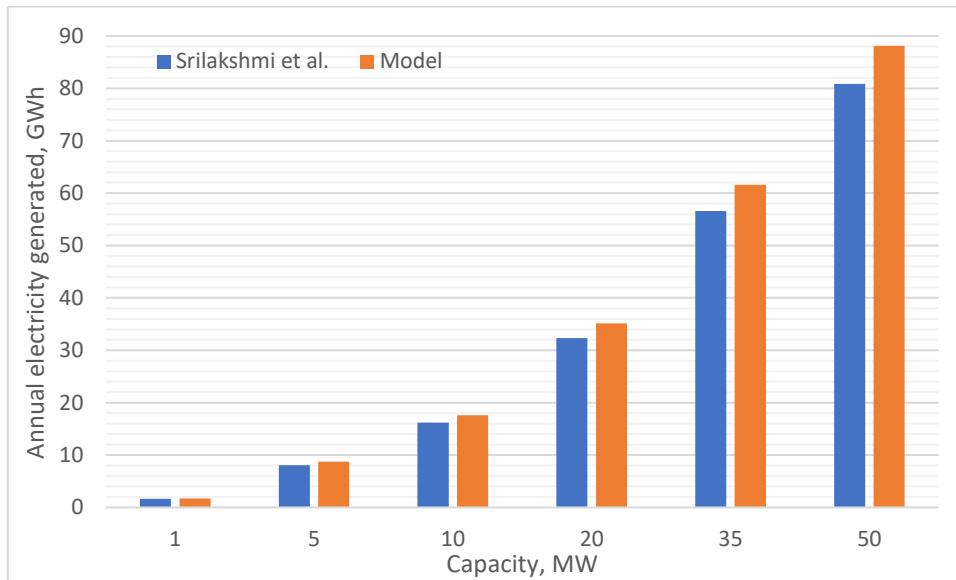

Figure 13 - Validation of the heliostat field model [43]

As it can be observed, the difference is small, below 10% in all compared cases, suggesting that the implementation of the model is correct. The most likely reason for this discrepancy is the inability to recreate the same conditions, mainly the year for which the simulation was performed and the exact location.

2.7. Desalination station

For the multi-effect distillation, a model suggested by Filippini et al. [55] was applied, with parts of the model by Darwish et al. [56]. The output of this model is the mass flow rate of the distillate obtained in the process as well as of the brine. The model is based on several assumptions:

A. it is a steady state process,

B. the vapour produced in each effect is completely salt free,

C. there are no losses to the environment,

D. heat transfer area is equal in all the effects,

E. pressure drops are neglected,

F. boiling point elevation and specific heat of seawater are a function of temperature and salinity,

G. latent heat of evaporation and overall heat transfer exchange coefficients are a function of temperature.

The functions for boiling point elevation, specific heat at constant pressure, latent heat of evaporation and global heat exchange coefficients are collected from [57] and are presented in Appendix A.
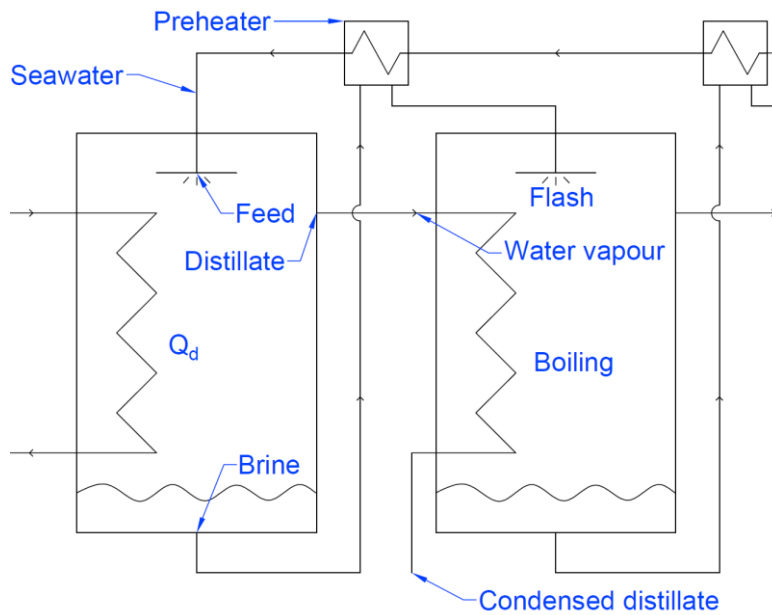

Figure 14 - Scheme of the first two effects

First, the temperature difference between two subsequent effects ΔT_d needs to be obtained. At this stage it is assumed to be constant throughout the system and later corrected. It is assumed to be 4°C, as the recommended minimum [4]. Based on the transformed formula for the temperature difference, the number of effects no_d can be calculated. Since it can only be an integer, the result is rounded down.

$$\Delta T_d = \frac{T_{d,1} - T_{d,B}}{no_d - 1} \tag{93}$$

$$no_d = \frac{T_{d,1} - T_{d,B}}{\Delta T_d} + 1 \tag{94}$$

where $T_{d,1}$ is the boiling temperature in the first effect, $T_{d,B}$ is the temperature of the brine from the last effect. The temperature difference in pre-heaters $\Delta T_{d,ph}$ is assumed to be equal to the temperature difference between the effects. The average temperature of the process $T_{d,mean}$ and the average salinity $x_{d,mean}$ is calculated as the arithmetic average between the first and last effect. Now, two parameters need to be evaluated. In each consecutive effect lower pressure than in previous one is maintained resulting in lower boiling temperature of water. As the brine collected from an effect enters the next one, due to the lower boiling

temperature part of the brine evaporates by flashing. The fraction of the brine rejected from the previous effect that is flashed in the next effect is denoted as α_d.

$$\alpha_d = \frac{c_p \cdot \Delta T_d}{\lambda_d} \tag{95}$$

where c_p is the specific heat at constant pressure and λ_d is the latent heat of evaporation. The specific heat is evaluated at the average temperature of the process, the latent heat of evaporation is evaluated at the same average temperature and the average salinity of the process. Another part of brine from previous effect evaporates by boiling. The fraction of the total distillate produced by boiling in each effect is denoted as γ_d.

$$\gamma_d = \frac{\alpha_d \cdot (x_{d,B} \cdot (1 - \alpha_d)^{no_d} - x_{d,F})}{(x_{d,B} - x_{d,F}) \cdot (1 - (1 - \alpha_d)^{no_d})} \tag{96}$$

where $x_{d,B}$ is the salinity of the brine from the final effect, $x_{d,F}$ is the feed (seawater) salinity. The temperature of the feed at the exit of the final condenser $T_{d,ph,fi}$ is assumed to be 11°C higher than the seawater temperature [55]. It is used to calculate the temperature of the feed for the first effect $T_{d,ph,1}$.

$$T_{d,ph,1} = T_{d,ph,fi} - (no_d - 1) \cdot \Delta T_{d,ph} \tag{97}$$

Now the mass flow rate of the feed $\dot{m}_{d,F}$ needs to be calculated. The heat delivered to the first effect by the heating water is known to be equal to 2 MW and is denoted as $\dot{Q}_d$. This heat is used to heat up the feed to the boiling temperature by sensible energy $\dot{Q}_{d,sens}$ and to vaporise a part of distillate by latent energy $\dot{Q}_{d,lat}$.

$$\dot{Q}_{d,sens} = \dot{m}_{d,F} \cdot \int_{T_{d,ph,1}}^{T_{d,1}} c_p \cdot dT \tag{98}$$

$$\dot{Q}_{d,lat} = \dot{m}_{d,D1} \cdot \lambda \tag{99}$$

where the latent heat of evaporation is obtained at the vapour temperature in the first effect $T_{d,v1}$ and $\dot{m}_{d,D1}$ is the mass flow rate of distillate from the first effect.

$$T_{d,v1} = T_{d,1} - BPE \tag{100}$$

$$\dot{m}_{d,D1} = \dot{m}_{d,D1,flash} + \dot{m}_{d,D1,boil} = \alpha_d \cdot \dot{m}_{d,F} + \gamma_d \cdot \dot{m}_{d,D} \tag{101}$$

$$\dot{m}_{d,D} = \dot{m}_{d,F} \cdot \frac{x_{d,B} - x_{d,F}}{x_{d,B}} \tag{102}$$

where BPE is the boiling point elevation estimated at the temperature in the effect and salinity, $\dot{m}_{d,D1,flash}$ is the mass flow rate of distillate flashed in the effect, $\dot{m}_{d,D1,boil}$ is the mass flow rate of the distillate boiled in the effect, $\dot{m}_{d,D}$ is the total mass flow rate of the distillate. Now the mass flow rate of the feed can be calculated. The formula is obtained by rearranging of an energy balance for the first effect.

$$\dot{Q}_d = \dot{Q}_{d,sens} + \dot{Q}_{d,lat} \tag{103}$$

$$\dot{Q}_d = \dot{m}_{d,F} \cdot \int_{T_{d,ph,1}}^{T_{d,1}} c_p \cdot dT + \left(\alpha_d \cdot \dot{m}_{d,F} + \gamma_d \cdot \dot{m}_{d,F} \cdot \frac{x_{d,B} - x_{d,F}}{x_{d,B}} \right) \cdot \lambda \tag{104}$$

$$\dot{m}_{d,F} = \frac{\dot{Q}}{\int_{T_{d,ph,1}}^{T_{d,1}} c_p \cdot dT + \left(\alpha_d + \gamma_d \cdot \frac{x_{d,B} - x_{d,F}}{x_{d,B}} \right) \cdot \lambda} \tag{105}$$

Mass flow rate of the brine from the first effect $\dot{m}_{d,B1}$ is calculated as the difference between the feed and the distillate.

$$\dot{m}_{d,B1} = \dot{m}_{d,F1} - \dot{m}_{d,D1} \qquad (106)$$

Since in this system forward feed is applied, for the first effect the mass flow rate of feed is equal to total mass flow rate of feed. Now the area of the heat transfer in the first effect is calculated. It is obtained by transforming an equation for the rate of heat transfer, with overall heat transfer coefficient $U_{d,ev1}$ - which is a function of temperature in the effect.

$$\dot{Q}_d = A_{d,ev1} \cdot U_{d,ev1} \cdot \Delta T_d \qquad (107)$$

$$A_{d,ev1} = \frac{\dot{Q}_d}{U_{d,ev1} \cdot \Delta T_d} \qquad (108)$$

Now that all the required parameters for the first effect are calculated, the same must be done for other effects. This part of the process requires an iterative approach. At this stage, the temperature difference between effects is assumed constant and calculated with equation (93). However, this assumption makes it impossible to fulfil assumption D. of the model – equal heat transfer area in all effects. After the first loop the areas are corrected to account for that, and all parameters are recalculated.

The temperature in effect k is calculated as the difference between the temperature in the previous effect and the difference of temperatures between the effects. The mass flow rate of the feed for an effect is equal to the mass flow rate of the brine from the previous effect. The mass flow rate of the distillate that is boiled is calculated with the coefficient γ_d and is equal for all effects; the mass flow rate of the distillate that is flashed in an effect is calculated as the product of coefficient α_d and mass flow rate of feed for that effect. The mass flow rate of brine is the difference between the feed and distillate.

$$T_{d,k} = T_{d,k-1} - \Delta T_d \qquad (109)$$

$$\dot{m}_{d,F,k} = \dot{m}_{d,B,k-1} \qquad (110)$$

$$\dot{m}_{d,D,boil,k} = \gamma_d \cdot \dot{m}_{d,d} \qquad (111)$$

$$\dot{m}_{d,D,flash,k} = \alpha_d \cdot \dot{m}_{d,F,i} \qquad (112)$$

$$\dot{m}_{d,D,k} = \dot{m}_{d,D,flash,k} + \dot{m}_{d,D,boil,k} \qquad (113)$$

$$\dot{m}_{d,B,k} = \dot{m}_{d,F,k} - \dot{m}_{d,D,k} \qquad (114)$$

The salinity in each effect needs to be calculated, as well as the thermal load.

$$x_{d,k} = \frac{x_{d,k-1} \cdot \dot{m}_{d,B,k-1}}{\dot{m}_{d,B,k}} \qquad (115)$$

$$\dot{Q}_{d,k} = \dot{m}_{d,D,boil,k-1} \cdot \lambda \qquad (116)$$

where the latent heat of evaporation is obtained at the temperature of the vapour in the effect. Temperature difference for the heat transfer in an effect $\Delta T_{d,ev,k}$ needs to be obtained. This is the difference between heat source for the effect (which is the vapour from the previous effect) and boiling temperature in the effect. With that, another formula for the thermal load in an effect can be applied, which upon transformation allows to calculate the heat transfer area.

$$\Delta T_{d,ev,k} = \left(T_{d,k-1} - BPE_{k-1}\right) - T_{d,k} = \Delta T_d - BPE_{k-1} \tag{117}$$

$$\dot{Q}_{d,k} = U_{d,ev,k} \cdot A_{d,ev,k} \cdot \Delta T_{d,ev,k} \tag{118}$$

$$A_{d,ev,k} = \frac{\dot{Q}_{d,k}}{U_{d,ev,k} \cdot \Delta T_{d,ev,k}} \tag{119}$$

Once those calculations are finished for every effect, the procedure to equalise the areas of the heat transfer needs to be implemented. Average area of heat transfer $A_{d,ev,mean}$ is calculated. New temperature difference for the heat exchange $\Delta T_{d,ev,k}$ is obtained from an equation for the thermal load.

$$A_{d,ev,mean} = \frac{\sum_{k=1}^{no_d} A_{d,ev,k}}{no_d} \tag{120}$$

$$\dot{Q}_{d,k} = U_{d,ev,k} \cdot A_{d,ev,mean} \cdot \Delta T_{d,ev,k} \tag{121}$$

$$\Delta T_{d,ev,k} = \frac{\dot{Q}_{d,k}}{U_{d,ev,k} \cdot A_{d,ev,mean}} \tag{122}$$

Now having applied the average area of heat exchange for all effects, the temperature difference between the effects is no longer fixed. New temperature profile for each effect is calculated.

$$\Delta T_{d,k} = \Delta T_{d,ev,k} + BPE_k \tag{123}$$

With the new temperature profile, the new temperature in every effect can be obtained, and all parameters including the temperature are recalculated. Finally, the new area of heat exchange is obtained for each effect. After each iteration, the difference in heat exchange areas is calculated.

$$\Delta A_{d,ev} = 100\% \cdot \frac{\max\left(A_{d,ev}(2:no_d)\right) - \min\left(A_{d,ev}(2:no_d)\right)}{A_{d,ev,mean}} \tag{124}$$

The first effect is exempted from this difference as it receives a different thermal load from the heating water. The process is repeated until the difference is below 1% and then the areas can be considered equal. The areas of the heat exchange are calculated for the average yearly temperature of the seawater. As the temperature changes over the year, upon fixing the areas, fresh water production in each month is calculated.

The distillate from the last effect needs to be condensed in the final condenser.
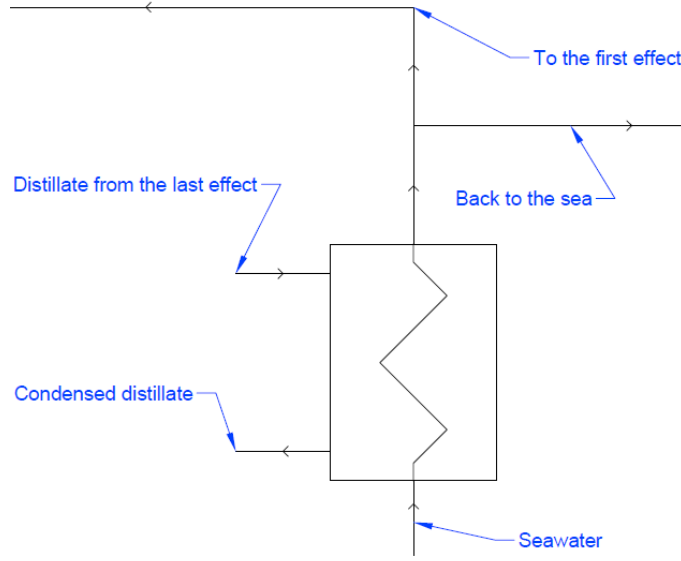
Figure 15 - Scheme of the final condenser

The area of that condenser $A_{d,cond}$, as well as required mass flow rate of seawater $\dot{m}_{d,sw}$ is calculated. The overall heat transfer coefficient of the condenser is obtained from a function, depending on the temperature in the final effect.

$$\dot{Q}_{d,cond} = \dot{m}_{d,D,fi} \cdot \lambda \tag{125}$$

$$\dot{Q}_{d,cond} = U_{d,cond} \cdot A_{d,cond} \cdot \Delta T_{d,log,cond} \tag{126}$$

$$\Delta\mathrm{T}_{d,log,cond} = \frac{T_{d,ph,fi} - T_{d,sw}}{\ln\left(\dfrac{T_{d,v,no_d} - T_{d,sw}}{T_{d,v,no_d} - T_{d,ph,fi}}\right)} \tag{127}$$

A different formula for the rate of heat transfer is applied, considering the mass flow rate of seawater, which upon transformation allows to obtain the required flow of seawater.

$$\dot{Q}_{d,cond} = \dot{m}_{d,sw} \cdot \int_{T_{d,sw}}^{T_{d,ph,f}} c_p \cdot dT \tag{128}$$

$$\dot{m}_{d,sw} = \frac{\dot{Q}_{d,cond}}{\int_{T_{d,sw}}^{T_{d,ph,f}} c_p \cdot dT} \tag{129}$$

Part of the mass flow rate of seawater is directed to the first effect as feed, and the rest is sent back to the sea.

2.7.1. Validation of the model

The described model was implemented in Python and the conditions from Filippini et al. [55] were recreated. The conditions are presented in Table 6. The simulation was performed for the desalination system with steam as the heat source for the first effect.

Table 6 - Conditions for the validation of the desalination model

Parameter	Value
Number of effects, -	10
Mass flow rate of steam, kg/s	5.67
Brine temperature, °C	40
Brine salinity, kg/m^3	60
Seawater temperature, °C	25
Seawater salinity, kg/m^3	39

The comparison was performed based on Gain Output Ratio GOR, which is used as a measure of performance for desalination plants. It is defined as the ratio of the quantity of distilled fresh water produced to the quantity of steam applied to the first effect [55]. The result for five different steam temperatures is presented in Figure 16.
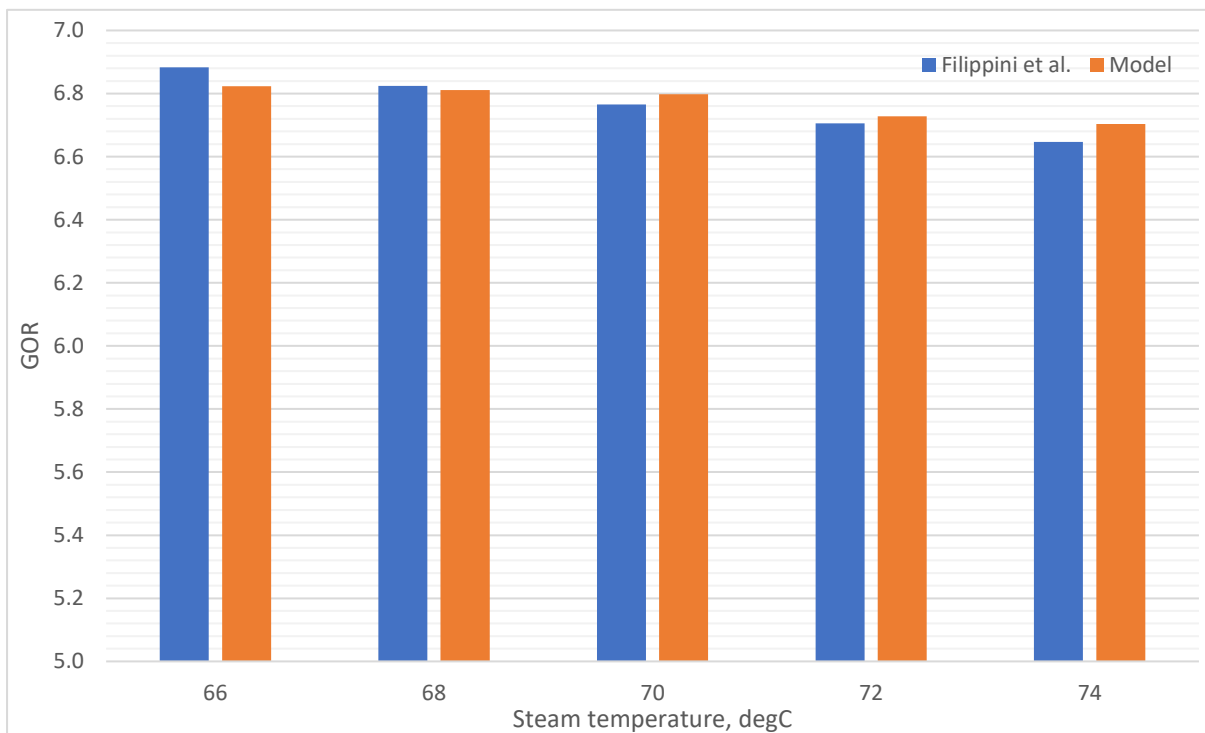

Figure 16 - Validation of the desalination system model [55]

As it can be observed, the obtained values are close to the ones from the paper, with errors not more than around 1.5%. This allows to conclude that the implementation of the model was correct.

2.8. Algorithm

As the model consists of many parts, in this section the order of calculations is shortly presented, along with the next steps of the analysis. First the efficiency of the heating water loop is calculated. As this efficiency is generally over 99% and does not present a significant change with the change of ambient temperature, it is assumed to

be constant throughout the year. The rest of the model requires calculation for every hour of the year, as it changes depending on certain factors.

Heliostat field is calculated following section 2.6. The weather data is provided in a CSV file [58] and prepared for the model – mainly not required parameters are removed. With solar power collected from the field in every hour, the efficiency of the central receiver can be calculated following section 2.5. Now, for each hour, the energy absorbed by the heat transfer fluid can be obtained.

$$P_{abs,i} = P_i \cdot \eta_{re,i} \tag{130}$$

It was also important to find the limits at which the system can operate. Generally, it is no more than 110% of the rated heliostat capacity and no less than 25% [43]. The reason for the upper limit is to avoid working in overload conditions, which could damage the equipment, and for the lower limit is to avoid excessive temperatures of the central receiver. With decreasing value of absorbed power the mass flow rate of the heat transfer fluid needs to be decreased to maintain its proper temperature. As a result, the surface temperature of the central receiver is increasing and could reach temperatures which the material could not withstand [40]. If it is not within these limits, the heliostats need to be defocused.

The next part concerns the storage system described in section 2.4. The level of HTF in the tank needs to be considered as it influences the efficiency of the tank. The mass of hot heat transfer fluid stored $m_{st,i}$ is calculated for every hour.

$$m_{st,i} = m_{st,i-1} + \left(\dot{m}_{st,inc,i} - \dot{m}_{st,out,i} \right) \cdot 3600s \tag{131}$$

where $\dot{m}_{st,inc,i}$ is the mass flow rate of the heat transfer fluid flowing from the central receiver in hour i, $\dot{m}_{st,out,i}$ is the mass flow rate of the heat transfer fluid leaving the storage and flowing to the heat exchanger. Since the mass flow rates are in $\frac{kg}{s}$, the difference is multiplied by 3600 to obtain the variation of the stored mass over one hour. The mass flow rate of the heat transfer fluid flowing to the heat exchanger is calculated from an energy balance of the heat exchanger.

$$\dot{m}_{st,out,i} = \frac{\dot{Q}_{hex}}{I_{htf,h,loss,i} - I_{htf,c}} \tag{132}$$

where $I_{htf,h,loss}$ and $I_{htf,c}$ are the specific enthalpies of the hot HTF (considering temperature decrease) and cold HTF, respectively. Due to losses from the storage tank, the temperature of the HTF inside may decrease. To consider that, the mass flow rate of heat transfer fluid that needs to be delivered to the heat exchanger is calculated for every hour of operation. The temperature considering the losses from the tank is obtained from the enthalpy and pressure inside the tank. The enthalpy is a result of an energy balance.

$$Q_{loss,i} = Q_{st,i-1} + \left(\dot{m}_{st,in,i} \cdot I_{htf,h} - \dot{m}_{st,out,i} \cdot I_{htf,loss} - \dot{Q}_{loss,st} \right) \cdot 3600s \tag{133}$$

$$I_{loss,i} = \frac{Q_{loss,i}}{m_{st.i}} \tag{134}$$

where $Q_{loss,i}$ is the energy stored considering the loss, $I_{loss,i}$ is the specific enthalpy in the tank after the loss. As this is an implicit equation – mass flow rate of HTF leaving the tank is depending on the losses - for the first hour temperature drop of 0.1K is assumed, and for next hours calculated temperature from the previous hour is

taken. If the difference between calculated and assumed temperature is above 1%, calculated value is used for the iteration. Generally, the difference is well below that and that assumption provides an accurate result while allowing to save computation time.

The mass flow rate of the heat transfer fluid flowing from the central receiver is calculated based on the power absorbed from the heliostat field.

$$\dot{m}_{st,in,i} = \frac{P_{abs,i}}{I_{htf,h} - I_{htf,c}} \tag{135}$$

If the temperature inside the cold tank decreases, the mass flow rate of HTF through the central receiver and heat exchanger needs to be lower to obtain design temperatures. This situation causes a problem for the process of calculations. Energy balance for the hot tank is dependent on the losses from the cold tank, whereas the energy balance for the cold tank is dependent on the losses from the hot tank. As the losses are changing based on the level in the tanks, they need to be calculated hourly. The process would be computationally expensive to find the balance of both tanks. Both are insulated to lower the losses, and considering the relatively low temperature of storage for the cold tank, as thermal oil and not molten salt is used, the losses from the cold tank are much lower than those from the hot tank. With that in mind, it is assumed that there are no losses from the cold tank. The losses from the hot tank are much more significant and for that the temperature drop is considered for the calculation of the mass flow rate to the heat exchanger. Neglecting the losses from the cold tank allows to save computation time in the already complex system.

The yearly sum of inflowing and outflowing mass flow rates is compared. If the outflow is above the inflow, it means that the system is not sustainable. Although the equivalent rated capacity considers efficiency of the system and average required storage time, the outcome depends on the weather conditions in the year. If the system is not sustainable, the capacity needs to be increased. The heliostat field can easily be adjusted by changing the height of the tower. In equation (89) the equivalent design capacity is increased by 0.5 MW and the process from that point repeats. This is the estimate as the losses from the tank are not known, so the capacity may also be recalculated later.

It is assumed that when the system is started in hour 0 of the year the heliostat field and storage has been operating before to fill the storage tank to a level required to maintain the continuous operation. The model finds the required amount of stored energy by comparing the inflow and outflow of the heat transfer fluid and finding a point where the level in the tank will be the lowest. Additionally, based on the point when the storage tank is filled to a highest point, the required height of the storage tank is calculated.

As the initial mass stored and height of the tank need to be known to start the computation of losses from the tank, for the first iteration it is assumed there are no losses from the hot tank. Additionally, the tank height is oversized by 10% to avoid it becoming completely full and initial mass stored by 5% to avoid the tank becoming completely empty. Later in the process of calculation of losses, if the level in the tank drops below 5% or level in the tank exceeds 99%, they need to be reassessed. If the level was too low, it means the initial mass was not sufficient so it is increased by 10%. If the tank becomes full, the height was too low so it is increased by 10%. With low level of fluid stored in tank the temperature decrease becomes more significant, which is why it should

not go below 5%. It also cannot become completely full as that is the assumption for the model of losses. Once the losses from the tank are calculated for the entire year, the final level in the tank is compared against the initial level. To make the system sustainable and avoid the tank becoming empty or full in the next year, the values should be similar. As no losses in the tank were assumed, the level at the end of the year may be lower. In that case, the capacity of the heliostat field is increased by 0.5 MW and calculations repeated from equation (89) – to recalculate the required height of the solar tower. The process is repeated until the difference in the levels does not exceed 20%. It would be possible to find more exact values, but that would increase the computation time significantly and as the weather conditions in the next year may change, there is no need for a perfect fit. Additionally, for the second and every next iteration an average temperature in the tank (including losses) is applied for estimate of dimensions, so the estimated values are closer to the real ones and allow to obtain the sustainability of the system faster.

Finally, the model of desalination is applied. The heat delivered to the first effect is constant, but the fresh water production is also dependent on other condition, namely the temperature of the sea water. As no data presenting hourly variation of that temperature is available, average monthly temperatures are used [59]. To find the design conditions of the plant, average yearly temperature is used. Then, for every month the amount of freshwater obtained is calculated considering the change of temperature.

The computational code presents the results in a form of a graph – the solar energy reflected by the field of heliostats over a year, the level to which the storage tank is filled, the amount of fresh water produced – and in the form of fixed values – the required height of the storage tank, the heliostat field capacity and the solar tower height. The results are presented in the next chapter. The algorithm is presented as flowchart in Figure 17.
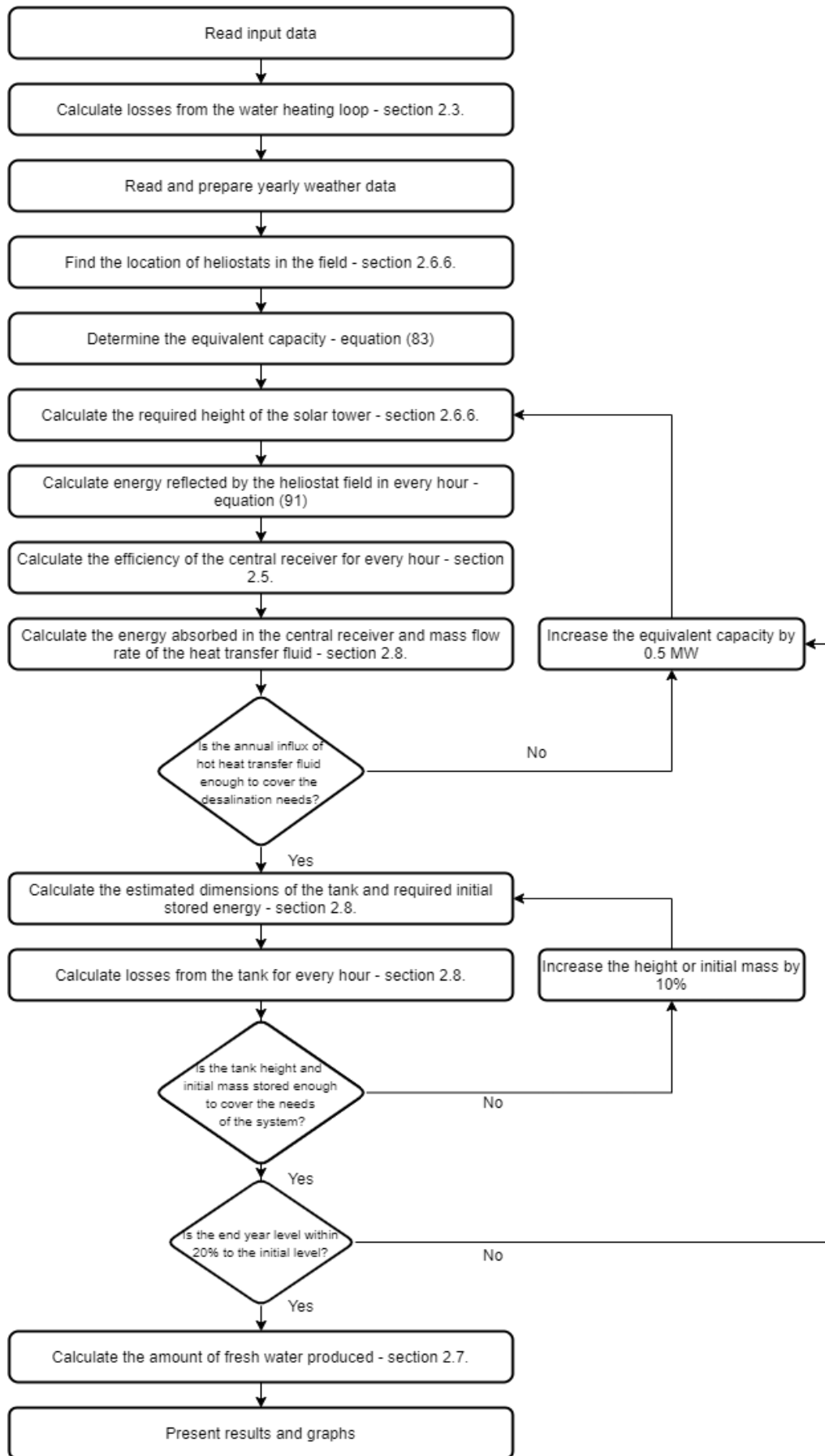
Figure 17 - Flowchart of the model

3. Results

3.1. Reference case

First, the simulation was performed under the reference set of input data, along with weather data for Jeddah in Saudi Arabia [58]. The set of data is delivered in a CSV file. The data along with their values and reference sources are presented in Table 7. The values for input parameters are either from the design data, assumptions or based on data from the literature.

Table 7 - Input data for the reference simulation

Parameter	Value	Reference
Location latitude, degrees	21.544	Design data
Heat transfer fluid		
Hot temperature, °C	300	[27]
Cold temperature, °C	75	[27]
Average pressure, Pa	151325	Assumed
Central receiver		
Tube outer diameter, m	0.019	[40]
Emissivity, -	0.8	[40]
Reflectivity, -	0.04	[40]
Tube thickness, m	0.00165	[40]
Insulation thickness, m	0.07	[40]
Design heat flux, kW/m^2	400	[40]
Desalination		
Capacity, kW	2000	Design data
Hot water temperature, °C	80	[56]
Cold water temperature, °C	60	[56]
Water pressure, Pa	111325	Assumed
Brine temperature, °C	40	[55]
Brine salinity, g/kg	60	[55]
Seawater salinity, g/kg	39.82	[20]
Storage		
Inner diameter, m	40	[37]
Wall thickness, m	0.006	[60]
Insulation thickness, m	1	[60]
Bottom insulation thickness, m	0.4	[37]
Heating water loop		
Tube diameter, m	0.4	Assumed
Tube wall thickness, m	0.005	Assumed

Tube length, m	10	Assumed
Insulation thickness, m	0.05	Assumed
Heat exchanger		
Shell internal diameter, m	2	Assumed
Shell wall thickness, m	0.05	Assumed
Shell insulation thickness, m	0.05	Assumed
Tube diameter, m	0.04	Assumed
Tube wall thickness, m	0.002	Assumed
Other		
Insulation conductivity, W/m^{2}K	0.043	[37]
Wall conductivity, W/m^{2}K	23.9	[40]
Insulation emissivity, -	0.6	[61]

As the process of calculation is composed of many steps, the program delivers a high number of results. For the presentation of the outcome of simulation, not all subsequent results are important, so they are not given here. Should it be necessary, they can be extracted from the model.

The key outcome is the production of fresh water from the desalination system. As it was already explained, due to lack of available data, only a monthly variation of temperature is assumed. The average monthly temperature of the seawater, presented in Figure 18, is used [59] and delivered in a CSV file. In Figure 19 the fresh water production over months can be observed. As for this analysis only the temperature of the seawater was changing over the months, it can be observed that the temperature has a strong influence on the outcome. In the summer months, when the temperature is higher, even about 20% more distillate can be obtained. The lowest value occurs in February, when the seawater temperature is the lowest. The boiling temperature in the first effect is maintained constant to assure proper operation of the system. As the temperature of the feed is higher, is it easier to bring it to the boiling temperature in the first effect and so the mass flow rate of the seawater can be higher. This results in higher feed also in subsequent effects (as in this case normal flow is analysed) and overall higher production of fresh water.
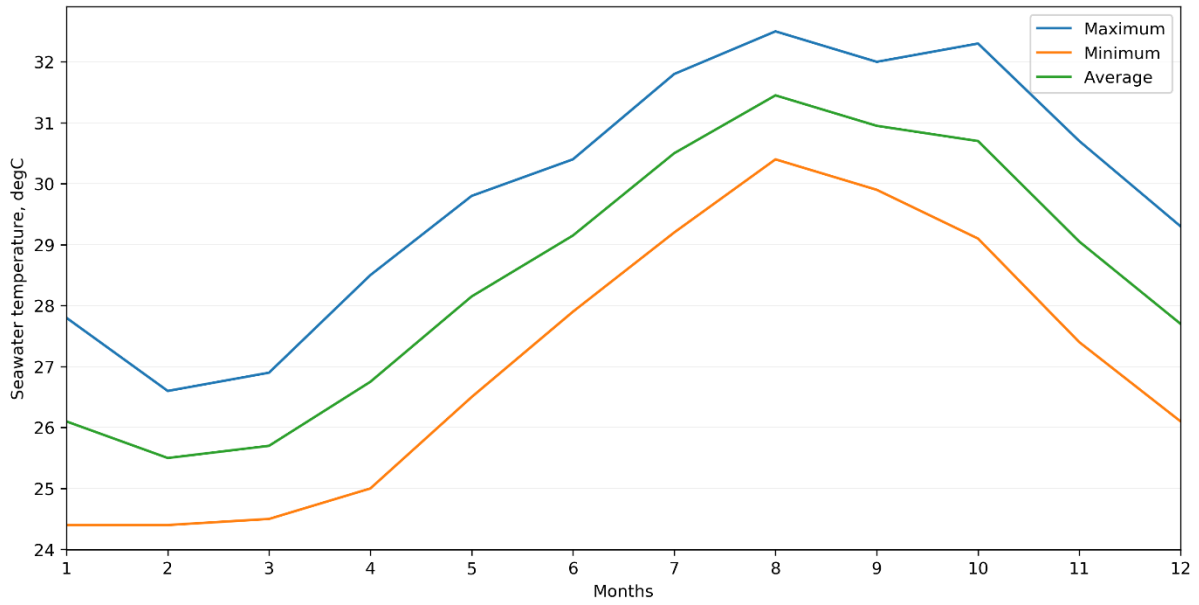
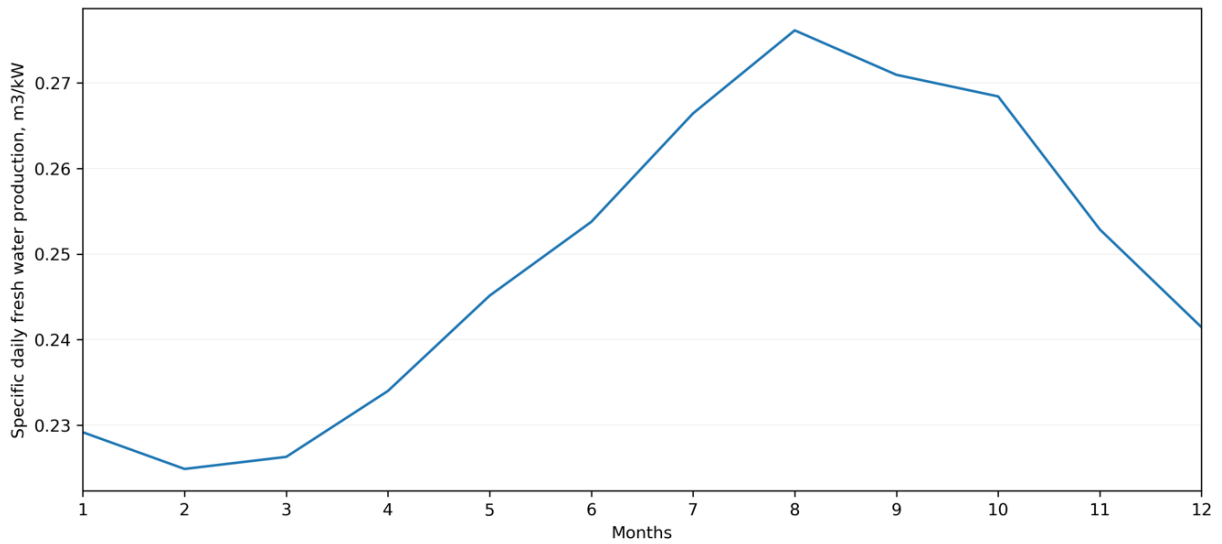*Figure 18 - Monthly variation of seawater temperature in the Red Sea*

Figure 19 - Fresh water production over months for the reference case

Figure 20 presents the salinity in the process of desalination. It is worth to note that the salinity of the feed entering the effects is presented, therefore for the first effect the salinity of the seawater, as in input data, is shown, and for final effect it is not equal to the salinity of the brine from input data. As expected, the feed becomes more and more concentrated, so the salinity is increasing throughout the system.
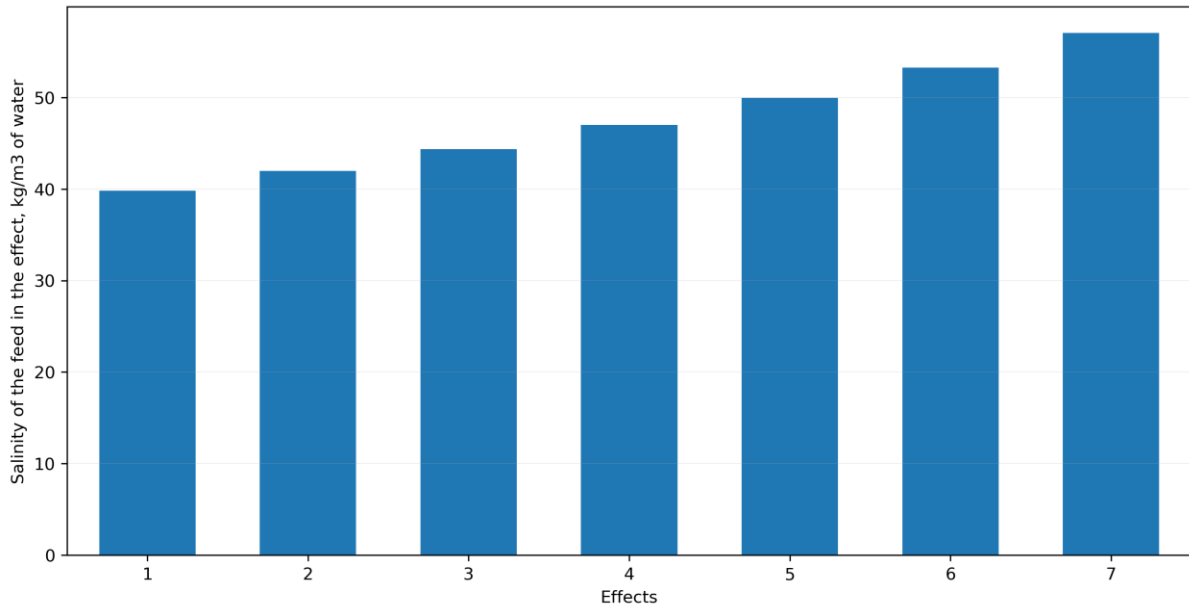
Figure 20 - Salinity in subsequent effects for the reference case

Figure 21 the distillate production in each effect for average yearly temperature of the seawater. As it was described in section 2.7, the distillate is obtained in two processes: flashing and boiling. Since the distillate from boiling for each effect is a fraction of total distillate in the applied model, the value is the same for each effect. For flashing, the distillate obtained is a fraction of the feed. As the feed is decreasing for each next effect, also the amount of distillate obtained from flashing is decreasing.
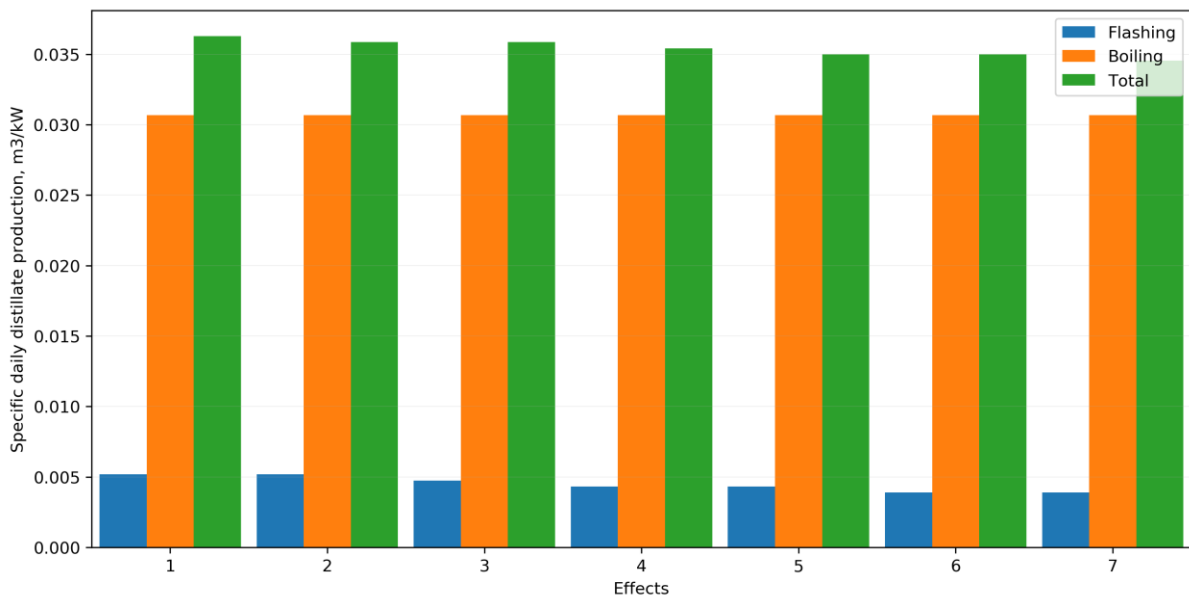

Figure 21 - Distillate production from subsequent effects for the reference case

To observe the behaviour of the CSP system throughout the year, two charts are presented. Figure 22 shows hourly solar power collected from the field and absorbed by the heat transfer fluid (considering the efficiency of the central receiver), and Figure 23, shows the level to which the storage tank is filled in every hour. As it can be observed, even though the location of the analysed plant is characterised by high DNI and generally good

weather conditions, the fluctuation of solar energy reflected by the heliostat field is still significant throughout the year. Also, the design power of the heliostat field is over five times higher than the power of the desalination plant. It is required due to efficiency of subsequent components and the requirement of storage to maintain continuous operation. The storage tank needs to be filled to a certain level before starting the system to roughly cover for the first three months of operation, where the DNI is lower than in later months due to the season of the year. The tank reaches its peak fill level around September, which is as expected, with it being the end of summer. Following the procedure described in section 2.8, the design capacity of the heliostat field is such that the end of the year level in the tank is similar as the initial level – in this case it is about 34% at the end to 37% at the beginning. Although the end of the year level is by a small degree lower than the one at the beginning, it is very close, and the system can be assessed as sustainable and expecting similar weather conditions in the next year the system is likely to maintain its continuous operation, without a need to stop the desalination system to refill the storage tank or a need to defocus the heliostats should the tank become completely full.
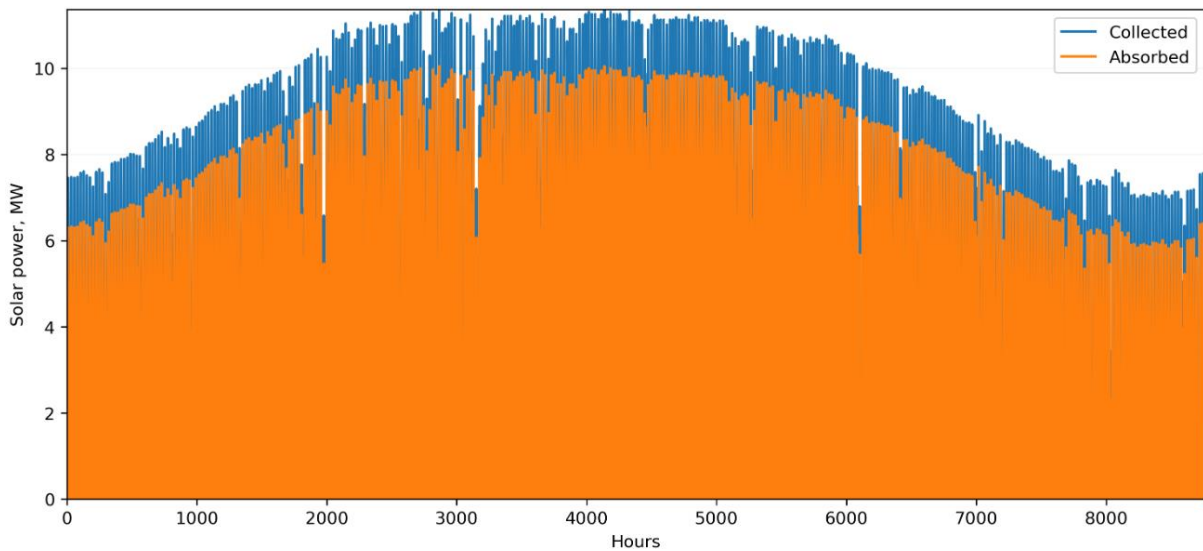

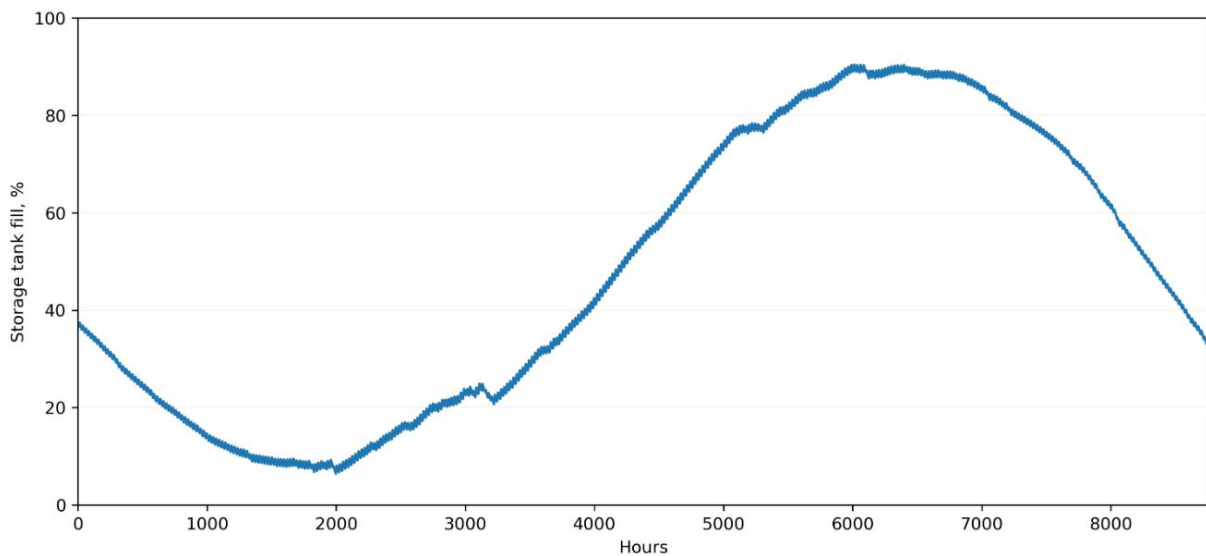*Figure 22 - Solar energy collected and absorbed over a year for the reference case*

Figure 23 – Hot tank storage fill level over a year for the reference case

The other crucial results which describe the system are the required design capacity of the heliostat field, required height of the tower and required height of the storage tank. Those results are presented in Table 8 and the further discussion is deferred to the next section.

Table 8 - Results from the reference case

Result	Value
Design power of the heliostat field, MW	11.3
Solar tower height, m	31.43
Storage tank height, m	16.96

3.2.   Second case

To observe the influence of location on the results, a second simulation was performed. All the inputs remained the same, only the location was changed – by changing the latitude and salinity [62] in input data along with a weather data file [58] and water temperature file [59]. The analysed location was Albufeira in Portugal. The results are compared and presented in Figure 24. As Portugal is characterised by lower DNI than Saudi Arabia, the design heliostat power needs to be higher to accommodate for the desalination plant requirements. As a result, the tower height is also increased, as it is mainly influenced by the design power of the field. With lower DNI, especially in the winter, during the summer months more hot HTF needs to be stored, resulting in a higher storage tank volume required. It is worth to note that generally storage tanks do not exceed a height of around 16 metres [63]. For Saudi Arabia, with height of around 17 metres it would most likely be possible to operate with one tank, but for Portugal, with calculated height of around 33 metres, at least two tanks would be required to store the heat transfer fluid.
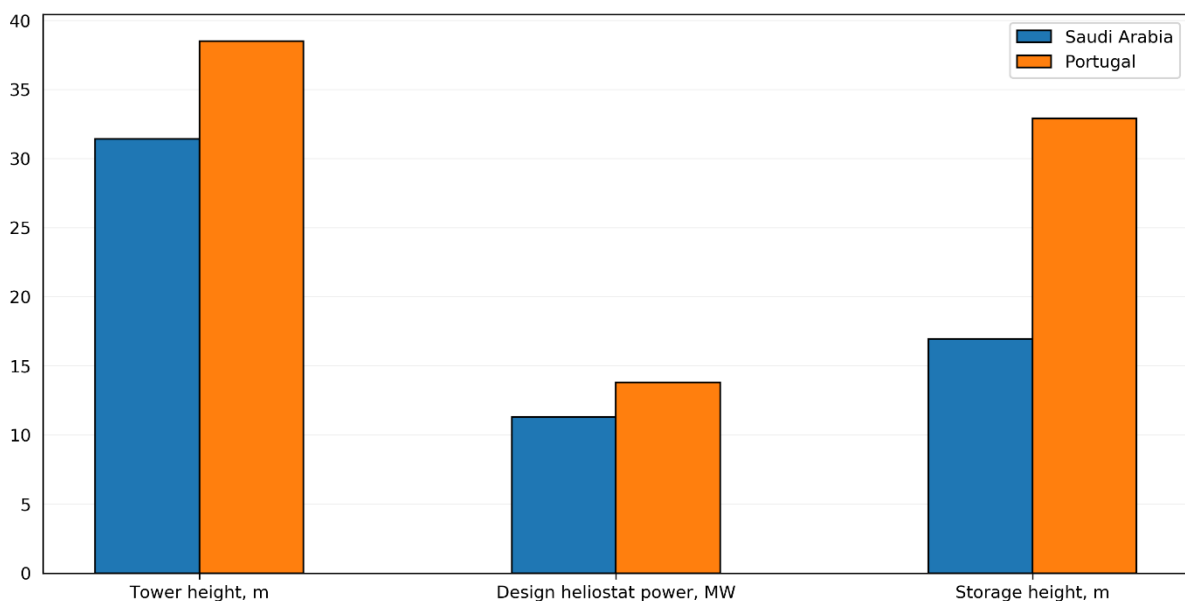

Figure 24 - Comparison of results for Saudi Arabia and Portugal

For more thorough comparison, yearly data presenting absorbed solar energy (Figure 25), amount of HTF stored (Figure 26) and variation of fresh water produced (Figure 27) are presented. Despite the higher design capacity

of heliostat field in Portugal, in the winter months still more solar energy is absorbed in Saudi Arabia due to higher DNI in those months. In summer, Portugal has higher level of absorbed energy due to the difference in design heliostat field power. The variation of absorbed energy over year is more significant in Portugal than in Saudi Arabia. As Saudi Arabia is located closer to the equator, the yearly change of DNI is smaller. It can also be observed that in Portugal interruptions in absorbed solar energy are more frequent. This is the result of operating limits of the central receiver, as it should not operate when the solar energy delivered to the receiver is below 25% of design capacity to avoid excessive temperatures on the surface of the receiver. As the design capacity of the heliostat field in Portugal is higher, during the winter months, with lower DNI, it is more frequent that the condition is not met and the heliostats need to be defocused. This issue could potentially be solved by altering the parameters of the receiver, as for this simulation only the location was changed and the design parameters were assigned with Saudi Arabia as location of the plant in mind.
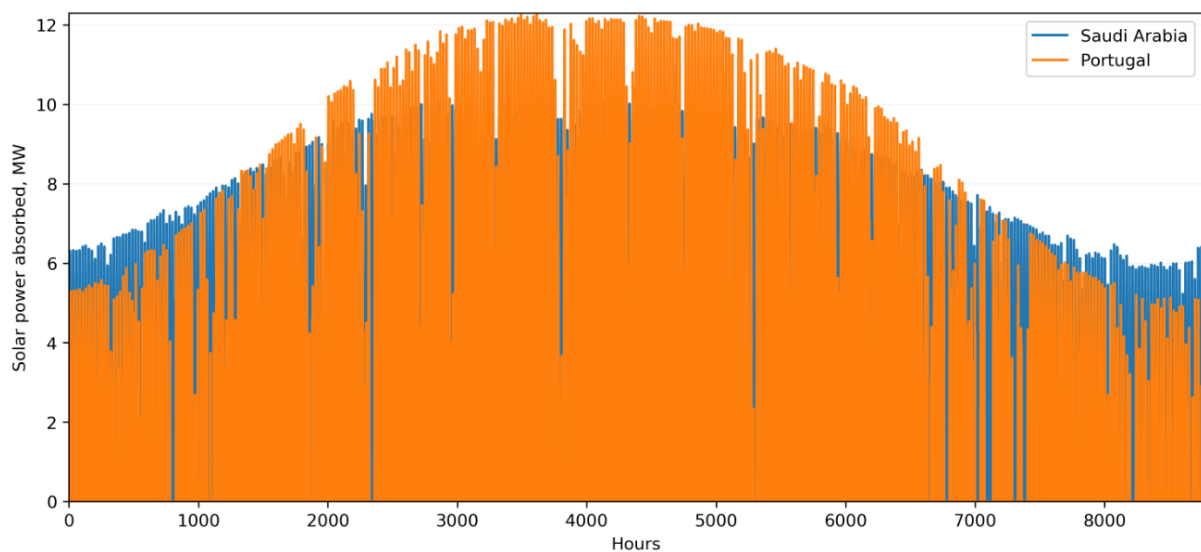

Figure 25 - Solar energy absorbed over a year in Saudi Arabia and Portugal

As the tanks are of different volume, here the absolute volume is used instead of percentage as in Figure 23. Due to lower DNI in the winter months, in Portugal it is necessary for the tank to start with a higher level of stored fluid. It reaches the lowest level about a month later than in Saudi Arabia, and after that reaches a much higher volume in the summer months. This high level is necessary to accommodate for the winter months. In both cases the level at the end of the year is similar to that at the begging of the year, so in both cases the system is sustainable. It can be noted that the minimum level in tank in Portugal is higher than in Saudi Arabia. This could indicate that the initial level in tank was oversized. As the initial level is a result of iterative process and it is increased by 10% once it is assessed as too low, it could lead to it being too high. Its accuracy could potentially be improved by changing the increment to 5%, but that would increase the computation time.
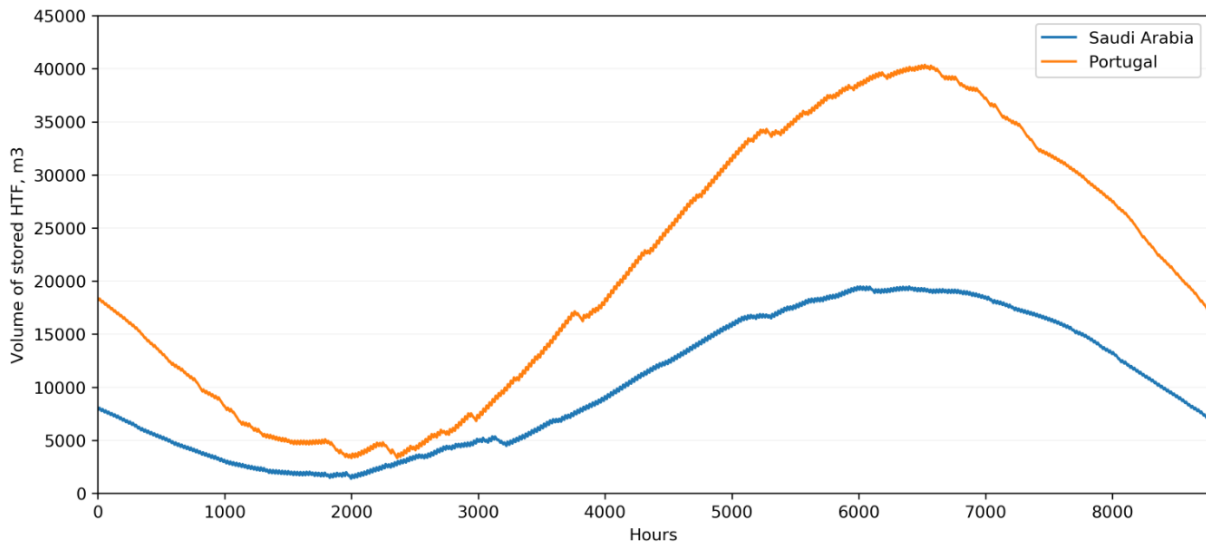
Figure 26 - Volume of stored HTF over a year in Saudi Arabia and Portugal

As it was already explained, a higher temperature of the seawater makes it easier to bring to the boiling temperature in the first effect, resulting in higher mass flow rate and distillate production. As the seawater temperatures in Portugal are lower, also the fresh water output is much lower. Although lower salinity increases the output, the temperature has much higher influence on the output and so it is not enough to offset the temperature difference. The tendency of both lines are similar – they are increasing in the summer months to reflect higher water temperature and decrease at the end of the year. Red Sea is characterised by higher variation of temperature over the year, so also the change of water production is greater.

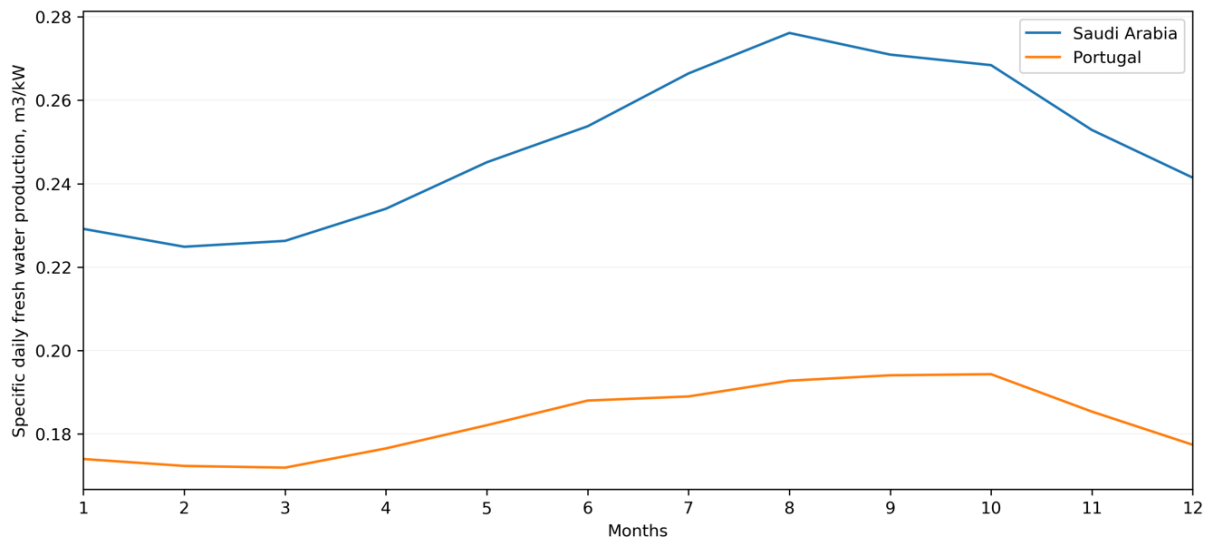*Figure 27 - Fresh water production over a year in Saudi Arabia and Portugal*

Overall it can be said that the conditions in Saudi Arabia are more favourable for the CSP Desalination system – due to higher DNI, lower variation of weather conditions over a year and higher seawater temperature. Those factors allow to use a heliostat field of lower design power, storage tank of lower volume and to produce more fresh water.

3.3. Parametric analysis

As the simulation requires over 30 input values, it can be useful to observe the behaviour of the system as they change, and to establish which are the most important. A set of simulations was performed, changing each of the input parameters presented in Table 7 (except for the first one, as the change of location was already analysed), one by one, first increasing by 10% and then decreasing by 10% relative to the refence case. Six results were observed, and their variation presented on graphs – capacity of the heliostat field in Figure 28, fresh water production in Figure 29, average temperature decrease in the hot storage tank in Figure 30, storage tank height in Figure 31 and yearly solar energy absorbed in the central receiver in Figure 32. If a parameter is not shown, it means it had no or marginal influence on the result.

Since for the design of the design heliostat field power an exact value is not found, but one that allows a close fit of storage tank level at the beginning and end of year in steps of 0.2 MW, a change of 10% of most inputs does not carry enough influence to require a different capacity. Four parameters that are important here are the design desalination power, the receiver emissivity, the receiver tubes diameter and the hot HTF temperature. Design desalination capacity is the base of sizing for the entire system and has an impact over the entire year, so it also has significant impact on heliostat capacity. Of the remaining three, only an increase of the parameter had enough influence to require a capacity alteration. Higher emissivity leads to lower efficiency of the receiver. Higher receiver tube diameter increases the flow area for the HTF and decreases the velocity of the flow. As a result, surface temperature of the receiver may be higher leading to greater heat losses from the receiver and thus requiring a higher capacity. Higher hot HTF temperature means more energy is required to obtain it. For the cold HTF its decrease does not impact the capacity as 10% of the hot HTF temperature is a greater absolute change than 10% of the cold HTF temperature. As the solar tower height is mainly dependent on the design capacity of the heliostat field, it is influenced by the same parameters and therefore a graph is not presented   here.
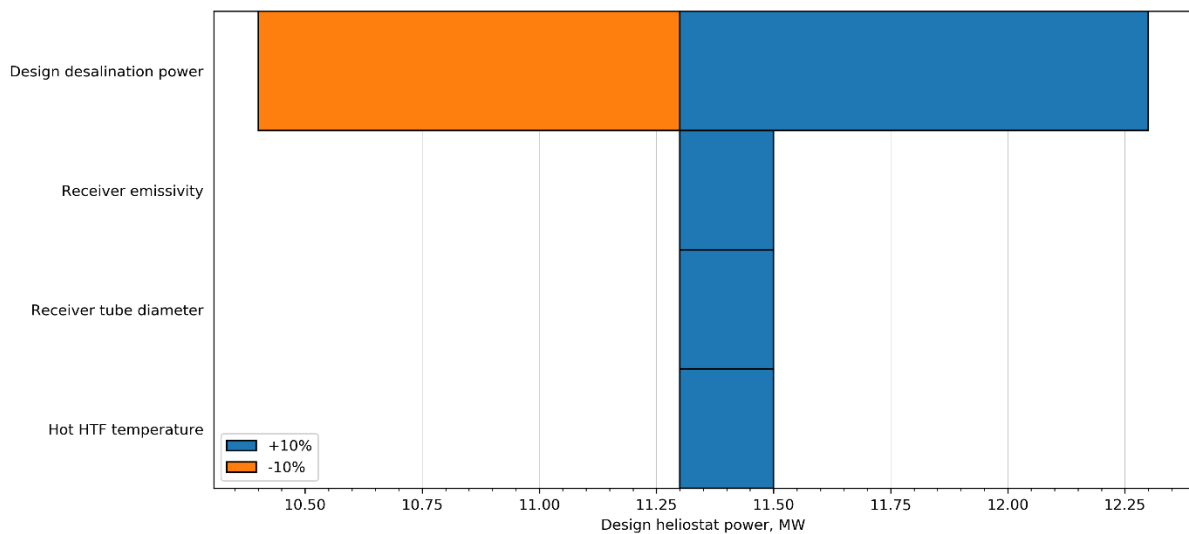

Figure 28 - Sensitivity analysis for design heliostat power

As it can be observed in Figure 29, there are four parameters which influenced the fresh water production. The most significant is the brine temperature, which can change the result by over 30%. Lower brine temperature means that the temperature of the last effect is lower, so with the fixed temperature of the first effect it means that the average temperature difference between effects is greater, making the heat exchange between subsequent effects more effective and resulting in higher distillate production. Changing the cold water temperature or hot water temperature influences the temperature in the first effect; if it is higher, the evaporation in this effect is more effective. However, it should be maintained at a proper value to avoid scaling and fouling problems, which may occur at higher temperatures. As expected, the design power also has a significant impact on the output. The decrease of seawater salinity or the increase of brine salinity has shown an increase of fresh water production, but with change of the salinity of only 10% the difference in the result was   marginal.
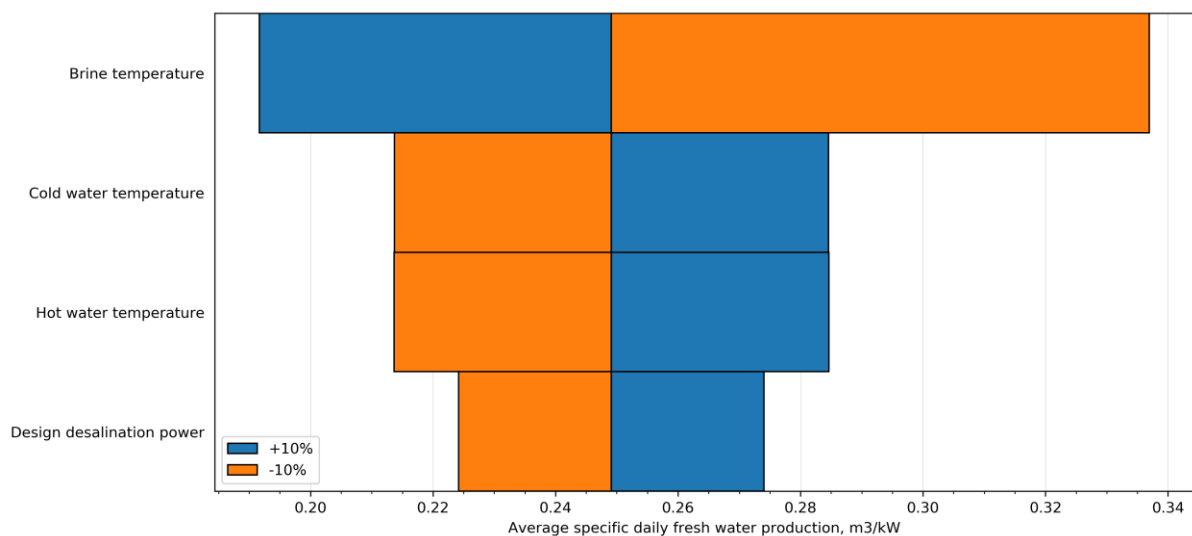

Figure 29 - Sensitivity analysis for fresh water production

Average temperature decrease in the hot tank, relatively to the reference case, is influenced by many parameters. The most significant one is the hot HTF temperature as it changes the temperature difference relative to the environment and thus strongly influencing the losses. It is worth to note that in the case of the hot HTF temperature, the receiver emissivity, the receiver tubes diameter and the design desalination power there is a strong asymmetry in the average temperature drop. This is because those inputs also require a change of the design power of the heliostat field, as shown in Figure 28, which generally has a great impact on the system and also on losses from the tank. Another parameter that yields strong asymmetry is the storage tank diameter. It influences the areas of heat loss – walls, top and bottom. As the relation between the diameter and the top or the bottom area is not linear, also the change in the average temperature drop is not symmetrical. As expected, the parameters related to the insulation – bottom and wall insulation thickness, its conductivity and emissivity all have influence on the result. Cold HTF temperature has a smaller role than most parameters, but it has impact on mass flow rate of the fluid leaving the storage tank and thus on the level of the fluid in the tank, which in turn influences the losses.
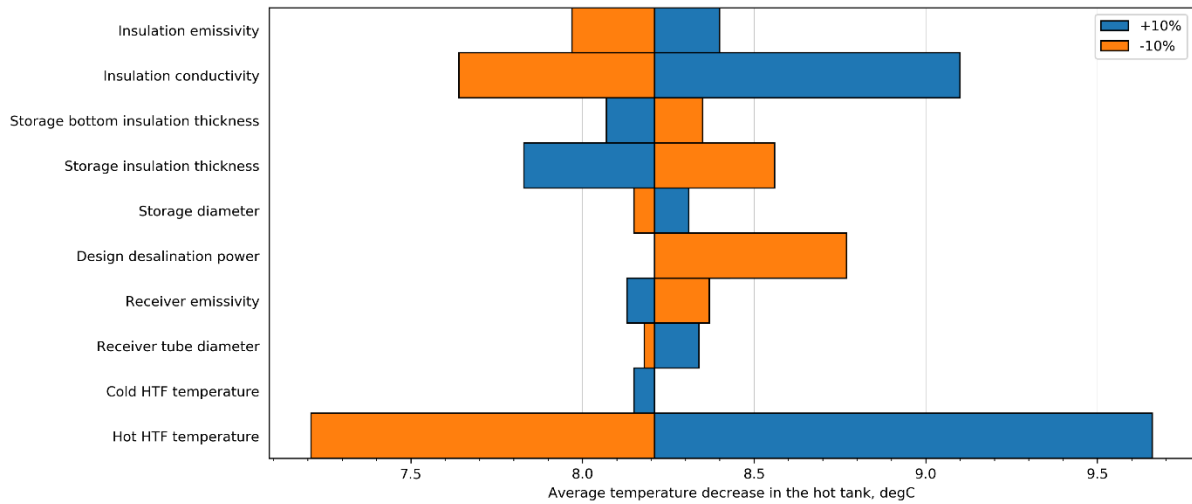
Figure 30 - Sensitivity analysis for average temperature decrease in the hot tank

The storage tank height is also influenced by many parameters. As the diameter is fixed (except for the case when it is the analysed parameter), whenever the required volume of the tank varies, the height needs to be changed. It is also related to the losses from the tank – higher losses mean the temperature in the tank is lower, mass flow rate of the fluid leaving the tank needs to be higher and thus the level in the tank decreases more rapidly. The most significant parameter is the storage diameter, as the volume of the tank is a function of diameter and height. The next one is the hot HTF temperature. With lower temperature the same amount of energy requires higher volume. With higher temperature lower volume is necessary; in this case also the results are asymmetrical as an increase of the hot HTF resulted in change of the heliostat design power. The same asymmetry can be observed with the receiver tubes diameter, the receiver emissivity and the design desalination power. The remaining parameters either influence the central receiver, thus reflecting on the mass flow rate of HTF incoming to the tank, or influence losses from the tank, thus changing the mass flow rate of the HTF leaving the tank. In both cases it means that different levels in the tank are reached. An interesting change worth mentioning is that insulation of lower thickness or greater conductivity allows to use a tank with smaller height. This is due to its influence on the losses from the tank. With greater losses more HTF needs to leave the tank resulting in the tank never becoming as full as with better insulation.
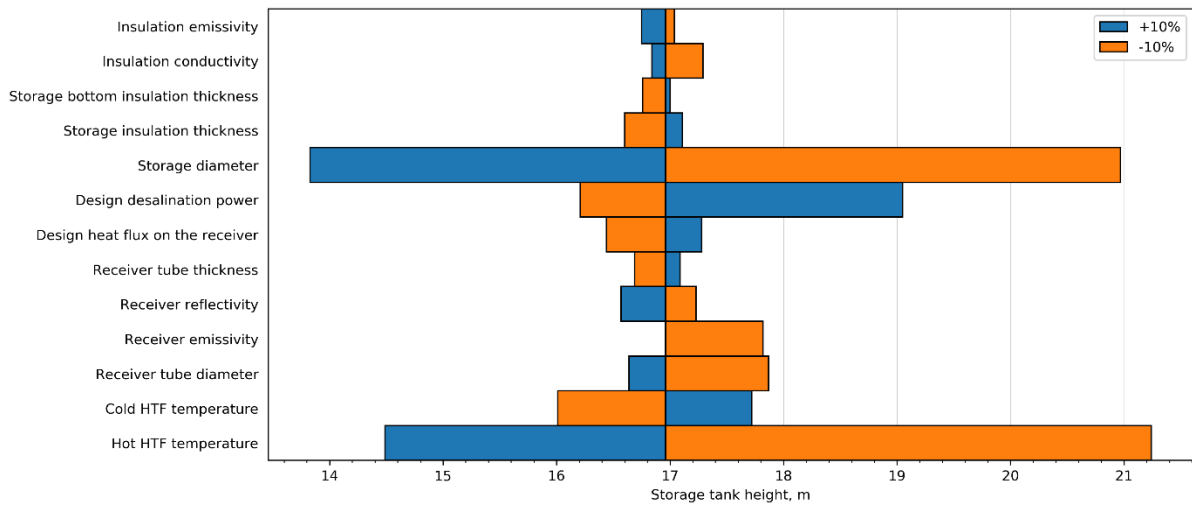
Figure 31 - Sensitivity analysis for storage tank height

The most significant impact on the yearly absorbed energy is caused by a change of the design power. As different design power requires larger or smaller capacity of the heliostat field, it will reflect on the yearly absorbed energy. The influence of the hot HTF temperature is asymmetrical as its increase requires higher capacity of the heliostat field. The decrease of the hot HTF temperature influences the operation of the central receiver and its efficiency, allowing for more energy to be absorbed. With lower hot HTF temperature the mass flow rate through the receiver can be increased, which decreases the surface temperature of the receiver and thus lowers the losses. The asymmetry in receiver emissivity and receiver tube diameter is also the result of the need to increase the design heliostat field power to accommodate for those changes. The other parameters which are present here influence the operation of the central receiver and its efficiency, thus increasing or decreasing the losses. Lower design heat flux on the receiver means that less energy can be absorbed. As the tubes diameter is fixed and the number of tubes must be an integer, in some cases the actual heat flux might differ from the design one, resulting in asymmetry of the outcome.
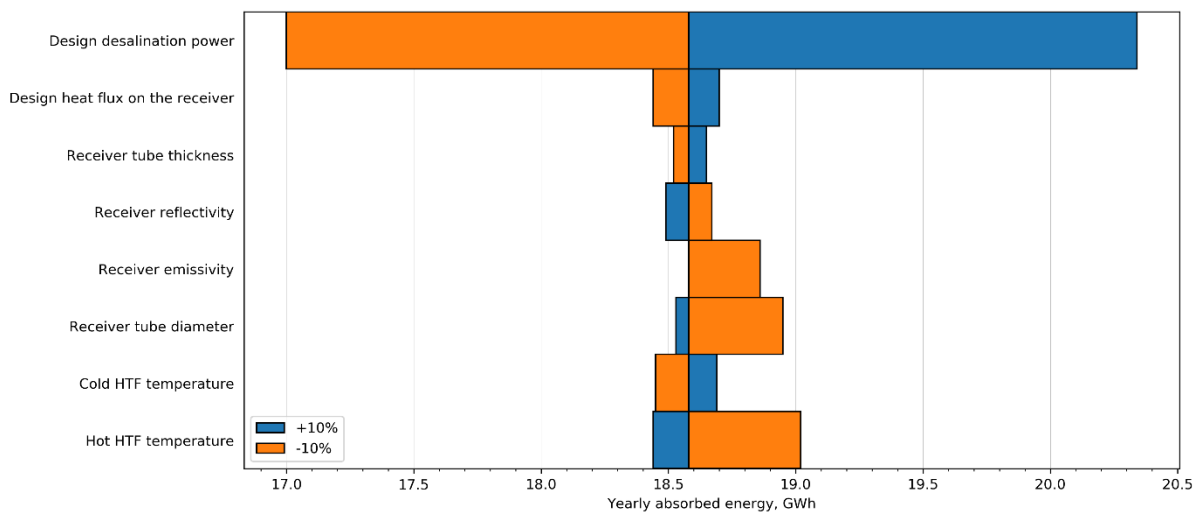

Figure 32 - Sensitivity analysis for yearly solar energy absorbed

54

Overall, the most significant parameter is the design power of the desalination system, as it is the base for the system and its change influences all the results. For desalination, temperature of brine, hot and cold water are especially important. For the tank volume and temperature decrease in the tank almost all parameters carry some influence, the most important being the temperature of the hot HTF fluid. For the energy absorbed, it is once again desalination capacity, along with the hot HTF temperature and followed by all parameters influencing the efficiency of the central receiver. The most important parameters for each subsystem are presented in Table 9.

Table 9 - The most important parameters for each subsystem

Subsystem	Main parameters
Heating water cycle	Hot and cold water temperature, insulation thickness
Thermal storage	Hot HTF temperature, insulation conductivity, design desalination power, storage insulation thickness
Central receiver	Receiver emissivity, receiver tube diameter, hot HTF temperature
Heliostats	Design desalination power, hot HTF temperature, receiver emissivity, receiver tubes diameter, DNI
Desalination station	Brine temperature, hot and cold water temperature, design desalination power

4. Conclusions

4.1. Work summary

The purpose of this thesis was to perform a thermodynamic analysis of a concentrated solar energy desalination plant. First, a review of existing technologies was performed, based on which the methods were chosen - solar tower with a storage system coupled with a multi-effect distillation. The system was divided into six parts: the heating water cycle, the storage system, the central receiver, the heliostats and the desalination plant. The model for each part was developed and then combined into one computational code. For the water heating cycle, it consisted of calculation of the heat losses to the environment from the pipes connecting the heat exchanger to the first effect of the desalination plant and from the heat exchanger. The storage system model also included heat losses to the environment, from three sources – the flat bottom surface of the tank, the walls of the tank and the flat top surface. The efficiency of the storage tank is especially important as the heat losses lead to a decrease of the temperature inside the tank. This results in a necessity to change the mass flow rate of the HTF leaving the tank to maintain proper temperature in other parts of the system. For better accuracy, these losses were calculated for every hour of operation to consider the variation of the mass flow rate and to observe the hourly level to which the tank is filled. For the central receiver, external type was chosen as best fit for the conditions. The heat losses due to convection, emission, reflection, and conduction were considered. To simplify the process of calculations, certain simplifications were applied, mainly the assumption that the temperature of fluid is constant in the entire receiver (taken as the average temperature between the inlet and outlet). The efficiency of the central receiver is dependent on the incoming solar energy from the heliostat field (and, to

smaller extend, on weather conditions), so it also had to be calculated for every hour of operation. The model of the heliostat field required arranging a theoretical heliostat field around the solar tower for the process of calculations and finding the proper locations of heliostats to obtain highest possible power with minimised losses. In this case also some simplifications had to be made, mainly with the reflective loss, the spillage loss and the shadowing and blocking loss. Their consideration is particularly complex, and it was decided that it is not necessary for this kind of analysis. The model for the desalination plant allows to calculate the amount of fresh water produced from the process based on the heat delivered from the heating water cycle. Each of the applied models was verified by comparing with the results from the literature, and all have indicated proper implementation.

The models were combined into one computational code which operates based on a CSV file containing input data and a CSV file with weather data for chosen year. The subsequent losses were calculated, with hourly calculation of the solar power reflected from the heliostat field, the corresponding efficiency of the central receiver, the losses from the thermal storage system and mass flow rates of the heat transfer fluid. The results of the thermodynamic analysis are thoroughly presented and discussed in section 3.

4.2. Main conclusions

It can be observed that although a concentrated solar energy desalination plant is a very interesting solution to the problem of limited fresh water resources, it is still dealing with some problems. The location of the analysed system was the Kingdom of Saudi Arabia, a region characterised by a high DNI throughout the year and a high water temperature. Even though the heat delivered to the desalination plant was constant, the variation of fresh water produced during the year was strong, changing by even about 20% from lowest to highest. The reason for that variation was the change of seawater temperature over months. A variable amount of fresh water produced from the system makes it less prone to be considered as a reliable source of fresh water. It would most likely be better to design the system with variable amount of heat delivered to the desalination plant, but with the aim of more consistent fresh water production. Despite a relatively high DNI the design heliostat field power still had to be over five times greater than the desalination plant to allow for a continuous operation. This means that a large area is required to place all the heliostats; the land area was considered as not important for the analysed location, as there are large desert areas available in Saudi Arabia, but if more plants were to be built it could eventually become an issue. Even though the yearly variation of DNI was not great in the analysed region, it still had impact on the solar power collected from the heliostat field and is especially noticeable when observing the change of the fill level in the storage tank. It reaches a low level in the winter months and becomes near full in the summer. It also must be of a great height to allow to store a high volume of the HTF. As a result, a big storage tank also means that the heat losses from it are becoming more severe. All those issues became even more apparent in the second analysed case, when the plant was moved to Albufeira in Portugal, where the average DNI is lower and its variation over a year is higher. Therefore, to minimise the impact of the issues related to the system, it is very important to analyse the location and the weather conditions associated with it. On the other hand, considering the other aspects, as Albufeira is a touristic city, during the winter months there are much fewer people and so also the fresh water demand is lower. Perhaps an alternative solution of disabling the

desalination plant for several months could be considered. Although the DNI in the winter is much lower, it would still allow to increase the level in the hot HTF storage tank if the desalination plant was not being used at all. As a result, also the design heliostat field power could be lower, along with lower dimensions of the storage tank, since the operation would be stopped in the winter.

Focusing on the observation of the performance of the system, it can be concluded that some parameters could be changed to optimize the operation. Although it is not within the scope of this thesis, a few interesting remarks can be made. For the desalination plant, a lower brine temperature for the final effect would allow to increase the fresh water production significantly. It would however be required to observe other parameters of the plant to assure its proper operation. A higher hot HTF temperature would allow to use a storage tank of lower height. On the other hand, it would require a greater design power of the heliostat field and would result in greater losses from the storage tank, so its insulation would need to be improved. Upon changing the location from Saudi Arabia to Portugal, an issue with the central receiver arose. In more cases the heliostat field had to be defocused as the surface temperature of the central receiver was too high and so the solar power could not be collected and absorbed at that time. It suggests that the geometrical design of the central receiver could be improved for that location. Although in Saudi Arabia that problem was not as common, perhaps it could also be improved for better overall performance of the system.

The aim when estimating the design power of the heliostat field was to make the system sustainable, so to have similar level in the tank at the beginning and at the end of the year. Although the end of the year level was a bit lower, overall the system was assessed as sustainable. It would be possible to find and exact fit to have the same levels, but it would increase the computation time significantly. Also, it would still be possible that in the next year the weather conditions will be so different that the heliostat field will need to be defocused once the tank becomes full or the desalination plant stopped should the tank become empty. With that in mind, the storage tank to a small degree oversized, and for the simulation is required to never become completely empty. Making the tank oversized and maintaining a certain level at all times makes the storage system more complex and more expensive, but it allows for more flexibility with the changing weather conditions. Finding the best design heliostat field power and tank dimensions could also be an issue for the optimization of the system. Analysing weather data for more than one year would give a better idea of what other weather conditions can be expected.

As the focus of this analysis was put on the thermal aspects of the system, some factors were not considered. The pressure losses occur due to flow and can be especially significant in the central receiver and heat exchanger, as those use tubes of small diameter. Another part of the system not included in the analysis are the pumps. They are used to maintain flow of the fluids, and in the desalination plant to maintain decreasing pressure in subsequent effects, which is the driving force for the flow of water and the evaporation process. The pumps use electrical energy, which was not considered in this analysis.

Overall, with the objective of this thesis being to analyse the thermodynamic cycle of the system and calculate the possible fresh water production along with the required heliostat field capacity, it can be assessed that the objective was fulfilled. Based on the presented graphs it can be concluded that the system is capable of

continuous operation. Although it was only observed for one year, looking at the end of the year HTF level in the tank, which is close to the one at the beginning of the year, the system can be assessed as sustainable.

4.3. Recommendations for future work

The future work on this model could include implementation of more complex calculations, mainly regarding the central receiver, where constant temperatures were assumed, and to the heliostat field, as some losses from that part are assumed constant and not calculated. Also, the pressure losses and the electrical energy requirements could be calculated.

As the system works based on a great number of input parameters, an optimization study could be performed to find the ways to improve the operation.

The operation of concentrated solar energy with desalination provides many possibilities in designing the system. Different components could be used, for example using molten salt instead of thermal oil, a cavity receiver instead of an external one or a reverse osmosis instead of a multi-effect distillation. Any of that could be implemented to see how it would affect the operation. An interesting option could be utilisation of fresh water storage – instead of maintaining a continuous operation of the desalination plant throughout the year, during summer months the high amount of fresh water produced could be stored and used in the winter months, where the production is lower.

The system could also be expanded by additional components, such as a heat pump or a chiller to utilise the heat in a more efficient way, a thermal vapour compression as an expansion of the multi-effect distillation or even combining generation of electricity along with the production of fresh water.

Bibliography

[1] A. Balasubramanian, "The World's Water," University of Mysore, Mysore, 2015.

[2] A. Eilmelech and W. A. Phillip, "The Future of Seawater Desalination: Energy, Technology and the Environment," *Science 333,* pp. 712-717, 2011.

[3] V. U. Patel and S. Multani, "A Review on Seawater Desalination Technology and Concentrating Solar Power," *International Research Journal of Engineering and Technology,* vol. 5, pp. 2669-2672, 2016.

[4] H. Zgeng, Solar Energy Desalination Technology, Beijing: Elsevier, 2017.

[5] A. Kassem, K. Al-Haddad and D. Komljenovic, "Concentrated solar thermal power in Saudi Arabia: Definition and simulation of alternative scenarios," *Renewable and Sustainable Energy Reviews,* vol. 80, pp. 75-91, 2017.

[6] L. G. Socaciu, "Thermal Energy Storage: An Overview," *Applied Mathematics and Mechanics,* vol. 55, pp. 785-794, 2012.

[7] A. G. Fernandez, H. Galleguillos, E. Fuentealba and F. J. Perez, "Thermal characterization of HITEC molten salt for energy storage in solar linear concentrated technology," *Journal of Thermal Analysis and Calorimetry,* vol. 122, pp. 3-9, 2015.

[8] F. Alnaimat and Y. Rashid, "Thermal Energy Storage in Solar Power Plants: A Review of the Materials, Associated Limitations, and Proposed Solutions," *Energies,* vol. 12, pp. 1-19, 2019.

[9] V. Belessiotis, S. Kalogirou and E. Delyannis, Thermal Solar Desalination: Methods and Systems, Elsevier, 2016.

[10] A. B. Pouyfaucon and L. Garcia-Rodriguez, "Solar thermal-powered desalination: A viable solution for a potential market," *Desalination,* vol. 435, pp. 60-69, 2018.

[11] H. Sharon and K. Reddy, "A review of solar energy driven desalination technologies," *Renewable and Sustainable Energy Reviews,* vol. 41, pp. 1080-1118, 2015.

[12] Y. Zhang, M. Sivakumar, S. Yang, K. Enever and M. Ramezanianpour, "Application of solar energy in water treatment processes: A review," *Desalination,* vol. 428, pp. 116-145, 2018.

[13] B. Ortega-Delgado, L. Garcia-Rodriguez and D. Alarcon-Padilla, "Thermoeconomic comparison of intergrating seawater desalination processes in a concentrating solar power plant of 5MWe," *Desalination,* vol. 392, pp. 102-117, 2016.

[14] M. Chandrashekara and A. Yadav, "Water desalination system using solar heat: A review," *Renewable and Sustainable Energy Reviews,* vol. 67, pp. 1308-1330, 2017.

[15] A. H. Hassabou, M. Spinnler and W. Polifke, "Tecnoeconomic analysis of medium and large-scale desalination plants driven by concentrated solar systems in the mena region," *Energy Procedia,* vol. 42, pp. 735-744, 2013.

[16] U. Jamil and W. Ali, "Performance tests and efficiency analysis of Solar Invictus 53S – A parabolic dish solar collector for direct steam generation," in *AIP Conference Proceedings 1734*, 2016.

[17] C. Kutscher, F. Burkholder and J. K. Stynes, "Generation of a Parabolic Trough Collector Efficiency Curve From Separate Measurements of Outdoor Optical Efficiency and Indoor Receiver Heat Loss," *Journal of Solar Energy Engineering,* vol. 134, p. 11012, 2012.

[18] E. J. Khalil, K. A. Munadhila and A. Kaysi, "The study of the performance and efficiency of flat linear Fresnel lens collector with sun tracking system in Iraq," *Renewable Energy,* vol. 14, pp. 41-48, 1998.

[19] O. P. Agboola, "The Potentials of Concentrating Solar Thermal Power in Meeting Saudi Future Energy Gap," in *World Congress on Engineering*, London, 2015.

[20] H. H. Omar, B. M. Abdullatif, M. M. El-Kazan and A. M. El-Gendy, "Red Sea Water and Biochemical Composition of Seaweeds at Southern Coast of Jeddah, Saudi Arabia," *Life Science Journal,* vol. 10, pp. 1073-1080, 2013.

[21] E. Zell, S. Gasim, S. Wilcox, S. Katamoura, T. Stoffel, H. Shibli, J. Engel-Cox and M. Al Subie, "Assessment of solar radiation resources in Saudi Arabia," *Solar Energy,* vol. 119, pp. 422-438, 2015.

[22] G. Van Rossum and F. L. Drake, Python 3 Reference Manual, Scotts Valley, CA: CreateSpace, 2009.

[23] C. R. Harris, K. J. Millman, S. J. van der Walt and et al., "Array programming with NumPy," *Nature,* vol. 585, pp. 357-362, 2020.

[24] I. H. Bell, J. Wronski, S. Quoilin and V. Lemort, "Pure and Pseudo-pure Fluid Thermophysical Property Evaluationand the Open-Source Thermophysical Property Library CoolProp," *Industrial and Engineering Chemistry Research,* vol. 53, pp. 2498-2508, 2014.

[25] W. McKinney, "Data Structures for Statistical Computing in Python," in *Proceedings of the 9th Python in Science Conference*, SciPy, 2010, pp. 56-61.

[26] J. D. Hunter, "Matplotlib: A 2D graphics environment," *Computing in Science & Engineering,* vol. 9, no. 3, pp. 90-95, 2007.

[27] "Therminol," Eastman, [Online]. Available: https://www.therminol.com/sites/therminol/files/documents/TF-8695_Therminol-66_Technical_Bulletin.pdf. [Accessed 02 2021].

[28] C. K. Ho, "Advances in central receivers for concentrating solar applications," *Solar Energy,* vol. 152, pp. 38-56, 2017.

[29] O. Behar, A. Khellaf and K. Mohammedi, "A review of studies on central receiver solar thermal power plants," *Renewable and Sustainable Energy Reviews,* vol. 23, pp. 12-39, 2013.

[30] C. K. Ho, "Advances in central receivers for concentrating solar applications," *Solar Energy,* vol. 152, pp. 38-56, 2017.

[31] Y. A. Çengel, Heat Transfer: A Practical Approach, 2003.

[32] V. Gnielinski, "New Equations for Heat and Mass Transfer in Turbulent Pipe and Channel Flow," *International Chemical Engineering,* vol. 16, pp. 359-368, 1976.

[33] B. S. Petukhov, "Heat Transfer and Friction in Turbulent Pipe Flow with Variable Physical Properties," *Advances in Heat Transfer,* vol. 6, pp. 503-564, 1970.

[34] S. W. Churchill and M. Bernstein, "A Correlating Equation for Forced Convection from Gases and Liquids to a Circular Cylinder in Cross Flor," *Journal of Heat Transfer,* vol. 99, pp. 300-306, 1977.

[35] S. W. Churchill and H. H. S. Chu, "Correlating Equations for Laminar and Turbulent Free Convection from a Vertical Plate," *International Journal of Heat Mass Transfer,* vol. 18, p. 1323, 1975.

[36] A. A. Abd and S. Z. Naji, "Analysis study of shell and tube heat exchanger for clough company with reselect different parameters to improve the design," *Case Studies in Thermal Engineering,* vol. 10, pp. 455-467, 2017.

[37] C. Suárez, F. J. Pino, F. Rosa and J. Guerra, "Heat loss from thermal energy storage ventilated tank foundations," *Solar Energy,* vol. 122, pp. 783-794, 2015.

[38] Y. Kurazumi, T. Tsuchikawa, J. Inshii, K. Fukagawa, Y. Yamato and N. Matsubara, "Radiative and convective heat transfer coefficients of the human body in natural convection," *Building and Environment,* vol. 43, pp. 2142-2153, 2008.

[39] P. Kosky, R. Balmer, W. Keat and G. Wise, Exploring Engineering, Elsevier, 2013.

[40] X. Li, W. Kong, Z. Wang, C. Chang and F. Bai, "Thermal model and thermodynamic performance of molten salt cavity receiver," *Renewable Energy,* vol. 35, pp. 981-988, 2010.

[41] M. A. Abaza, W. M. El-Maghlany, M. Hassab and F. Abulfotuh, "10 MW Concentrated Solar Power (CSP) plant operated by 100% solar energy: Sizing and techno-economic optimization," *Alexandria Engineering Journal,* vol. 59, pp. 39-47, 2020.

[42] P. K. Falcone, "A handbook for solar central receiver design," Sandia National Labs, Livermore, CA, USA, 1986.

[43] G. Srilakshmi, M. A. Ramaswamy and N. C. Thirumalai, Design of Solar Field and Performance Estimation of Solar Tower Plants, CSTEP, 2016.

[44] F. Eddihibi, "Optical study of solar tower power plants," *Journal of Physics: Conference Series,* vol. 596, 2015.

[45] A. J. Gutiérrez-Trashorras, E. Villicaña-Ortiz, E. Álvarez-Álvarez, J. M. González-Caballín, J. Xiberta-Bernat and M. J. Suarez-López, "Attenuation processes of solar radiation. Application to the quantificationof direct and diffuse solar irradiances on horizontal surfaces in Mexicoby means of an overall atmospheric transmittance," *Renewable and Sustainable Energy Reviews,* vol. 81, pp. 93-106, 2018.

[46] M. Schmitz, P. Schwarzbozl, R. Buck and R. Pitz-Paal, "Assessment of the potential improvement due to multiple apertures in central receiver systems with secondary concentrators," *Solar Energy,* vol. 80, pp. 111-120, 2006.

[47] C. J. Noone, M. Torrilhon and A. Mitsos, "Heliostat field optimization: A new computationally efficient model and biomimetic layout," *Solar Energy,* vol. 86, pp. 792-803, 2012.

[48] Y. Zhou and Y. Zhao, "Heliostat Field Layout Design for Solar Tower Power Plant Based on GPU," *IFAC Proceedings Volumes,* vol. 47, pp. 4953-4958, 2014.

[49] F. J. Collado, "Quick evaluation of the annual heliostat field efficiency," *Solar Energy,* vol. 82, pp. 379-384, 2008.

[50] F. J. Collado and J. A. Turegano, "Calculation of the annual thermal energy supplied by a defined heliostat field," *Solar Energy,* vol. 42, pp. 149-165, 1989.

[51] Z. A. Hussaini, P. King and C. Sansom, "Numercial Simulation and Design of Multi-Tower Concentrated Solar Power Fields," *Sustainability,* vol. 12, p. 2402, 2020.

[52] F. J. Collado and J. Guallar, "A review of optimized design layouts for solar power tower plants with campo code," *Renewable and Sustainable Energy Review,* vol. 20, pp. 142-154, 2013.

[53] L. Garcia, M. Burisch and M. Sanchez, "Spillage estimation in a heliostat field for solar field optimization," *Energy Procedia,* vol. 69, pp. 1269-1276, 2015.

[54] C. J. Noone, M. Torrilhon and A. Mitsos, "Heliostat field optimization: A new computationally efficient model and biomimetic layout," *Solar Energy,* vol. 86, no. 2, pp. 792-803, 2012.

[55] G. Filippini, M. A. Al-Obaidi, F. Manenti and I. M. Mujtaba, "Performance analysis of hybrid system of multi effect distillation and reverse osmosis for seawater desalination via modeling and simulation," *Desalination,* vol. 448, pp. 21-35, 2018.

[56] M. A. Darwish, F. Al-Juwayhel and H. K. Abdulraheim, "Multi-effect boiling systems from an energy viewpoint," *Desalination,* vol. 194, pp. 22-39, 2006.

[57] H. T. El-Dessouky and H. M. Ettouney, Fundamentals of salt water desalination, Elsevier, 2002.

[58] European Comission, "Photovoltaic Geographical Information System (PVGIS)," [Online]. Available: https://ec.europa.eu/jrc/en/pvgis. [Accessed May 2021].

[59] "SeaTemperature," [Online]. Available: https://www.seatemperature.org/. [Accessed May 2021].

[60] X. Zhang, Y. Wu, C. Ma, Q. Meng, X. Hu and C. Yang, "Experimental Study on Temperature Distribution and Heat Losses of a Molten Salt Heat Storage Tank," *Energies,* vol. 12, p. 1943, 2019.

[61] P. Corning, FOAMGLAS Industrial Insulation Handbook, Waterloo, Belgium: Editions Technip, 1992.

[62] A. Peliz, J. Dubert, P. Marchesiello and A. Teles-Machado, "Surface circulation in the Gulf of Cadiz: Model and mean flow structure," *Journal of Geophysical Research,* vol. 112, 2007.

[63] U. Herrmann, "Two-Tank Molten Salt Storage for Parabolic Trough Solar Power Plants," *Energy,* vol. 29, pp. 883-293, 2004.

[64] F. W. Dittus and L. M. K. Boelter, "University of California Publications on Engineering 2," p. 433, 1930.

[65] J. Kim, J. S. Kim and W. Stein, "Simplified heat loss model for central tower solar receiver," *Solar Energy,* vol. 116, pp. 314-322, 2015.

[66] J. Coventry and J. D. Pye, "Heliostat Cost Reduction - Where to Now?," *Energy Procedia,* vol. 49, pp. 60-70, 2013.

[67] D. L. Siebers and J. S. Kraabel, "Estimating Convective Energy Losses From Solar Central Receivers," Sandia National Laboratories, Livermore, 1984.

[68] A. Zukauskas, "Convection Heat Transfer in Cross Flow," *Advances in Heat Transfer,* vol. 8, pp. 93-106, 1972.

[69] G. Colomer, J. Chiva, O. Lehmkuhl and A. Oliva, "Advanced CFD&HT numerical modeling of solar tower receivers," *Energy Procedia,* vol. 49, pp. 50-59, 2014.

[70] A. Hatzikioseyian, R. Vidali and P. Kousi, "Modelling and Thermodynamic Analysis of a Multi Effect Distillation (MED) Plant for Seawater Desalination," National Technical University of Athens (NTUA), Athens, Greece, 2004.

[71] "Foamglas Insulation Systems," FOAMGLAS, [Online]. Available: https://cjmetalerectors.com/wp-content/themes/zidex-child/pdf/DATA-FOAM-Foamglas%20Installation.pdf. [Accessed May 2021].

[72] G. Zanganeh, A. Pedretti, S. Zavattoni, M. Barbato and A. Steinfeld, "Packed-bed thermal storage for concentrated solar power – Pilot-scale demonstration and industrial-scale design," *Solar Energy,* vol. 86, pp. 3084-3098, 2012.

[73] A. Omar, A. Nashed, Q. Li, G. Leslie and R. A. Taylor, "Pathways for integrated concentrated solar power - Desalination: A critical review," *Renewable and Sustainable Energy Reviews,* vol. 119, pp. 1096-1109, 2020.

[74] X. Py, N. Sadiki, R. Olives, V. Goetz and Q. Falcoz, "Thermal energy storage for CSP (Concentrating Solar Power)," *The European Physical Jorunal Conferences,* vol. 148, 2017.

[75] Y. A. Alamri, S. Mahmoud, R. Al-Dadah, S. Sharma, J. N. Roy and Y. Ding, "Optical Performance of Single Point-Focus Fresnel Lens Concentrator System for Multiple Multi-Junction Solar Cells - A Numerical Study," *Energies,* vol. 14, p. 4301, 2021.

Appendices

Appendix A: the functions for boiling point elevation, specific heat at constant pressure, latent heat of evaporation and global heat exchange coefficients [57]

$$BPE_a = 8.325 \cdot 10^{-2} + 1.883 \cdot 10^{-4} \cdot T + 4.02 \cdot 10^{-6} \cdot T^2$$

$$BPE_b = -7.625 \cdot 10^{-4} + 9.02 \cdot 10^{-5} \cdot T - 5.2 \cdot 10^{-7} \cdot T^2$$

$$BPE_c = 1.522 \cdot 10^{-4} - 3 \cdot 10^{-6} \cdot T - 3 \cdot 10^{-8} \cdot T^2$$

$$BPE = BPE_a \cdot sal + BPE_b \cdot sal^2 + BPE_c \cdot sal^3$$

$$cp_a = 4206.8 - 6.6197 \cdot sal + 1.2288 \cdot 10^{-2} \cdot sal^2$$

$$cp_b = -1.1262 + 5.4178 \cdot 10^{-2} \cdot sal - 2.2719 \cdot 10^{-4} \cdot sal^2$$

$$cp_c = 1.2026 \cdot 10^{-2} - 5.3566 \cdot 10^{-4} \cdot sal + 1.8906 \cdot 10^{-6} \cdot sal^2$$

$$cp_d = 6.8777 \cdot 10^{-7} + 1.517 \cdot 10^{-6} \cdot sal - 4.4268 \cdot 10^{-9} \cdot sal^2$$

$$cp = \frac{cp_a + cp_b \cdot T + cp_c \cdot T^2 + cp_d \cdot T^3}{1000}$$

$$U_{ev} = 1.9695 + 1.2057 \cdot 10^{-2} \cdot T - 8.5989 \cdot 10^{-5} \cdot T^2 + 2.2651 \cdot 10^{-7} \cdot T^3$$

$$U_{cond} = 1.7194 + 3.2063 \cdot 10^{-3} \cdot T + 1.597 \cdot 10^{-5} \cdot T^2 - 1.9918 \cdot 10^{-7} \cdot T^3$$